Computational Solid Mechanics Laboratory LSMS

Semester Project

Bachelor/Master pre-study project
Exploration of auxetics materials in sport

Authors:
Thibault Ghesquière-Diérickx and Nicolas Tireford

With help of:
Jean-François Molinari, Son Pham-Ba, Sacha Wattel, John Kolinski, Ghatu Subhash and Youssef Eddebbarh

Synthesis
A special property of auxetic materials is their negative Poisson's ratio : this material shortens or lengthen in all directions when subjected respectively to a compressive or tensile force. This unusual characteristic opens up new perspectives in many fields. Sport is one of the fields where these properties can be well exploited. Already studied and already used for protective equipment, their properties could also prove themselves useful with other application such as grips. The goal of this paper is to study the properties of a sole cell, modelled to exhibit the auxetic behaviour, although the material itself is not auxetic. 3D modelling will allow both parametric finite element studies and the possibility of making 3D prints for testing friction especially.

June 17, 2021

Contents

1 Introduction

Auxetic materials are greatly studied and analysed. They offer unusual properties that open up new possibilities in various fields, whether it is in robotics, medicine or sports. In recent years, studies started to go into greater depth and auxetic materials are emerging as an opportunity, an investment in the future.
In the sport field, this new type of material is more about shock absorption than it is about grip and friction which could be applied in numerous sports, from overgrips on tennis rackets, to running shoe soles. In 2016, Nike released a running shoe composed of an auxetic sole, that supposedly enables an athlete's natural motion and allow the foot to be in control rather than the shoe [1].

By understanding what are auxetic materials, it will be possible to study the Nike auxetic shoe sole patent [2], the different paramaters of the cell and how they dictate the sole behaviour. The idea is to model, with the help of 3D software, the structure of an auxetic sole. This will allow finite element studies to be carried out, but also the printing of 3D samples and the study of their real behaviour. The initial goal is to see if the desired auxetic behaviour is present, both in theory with finite elements method FEM and in practice. Moreover, the possibilities these materials offer, for example in terms of friction, are interesting to study. With a parametric 3D model, it will be possible to vary the different parameters of an auxetic sole in order to see the characteristics that will give the optimal auxetic behaviour to the running shoe.
This work is only a preliminary study of the possibilities offered by the auxetic shoe sole. However, it presents a more precise idea of their functioning and of their behaviour.

2 Preliminary studies

2.1 Types of auxetic structure

Poisson's ratio ν is the measurement that characterizes the Poisson effect of a material. When a load is applied on a material, it will deform in the direction of loading ϵ_{axial} but also in the perpendicular direction ϵ_{trans}. Under a compression load, usual materials tend to contract in the loading direction and expand in the perpendicular direction. The Poisson's ratio $\nu = -\epsilon_{trans}/\epsilon_{axial}$ ranges between 0 to 0.5. Auxetics are structure or materials that exhibit a negative Poisson's ratio. This unusual behaviour is characterized by special nano/micro- or macrostructures. If subjected to compression, an auxetic material will shorten in all directions; that is the direct consequence of the typology of their architecture. Three main types of structure allow that auxetic behaviour [3]. The features of these different typologies are presented below.

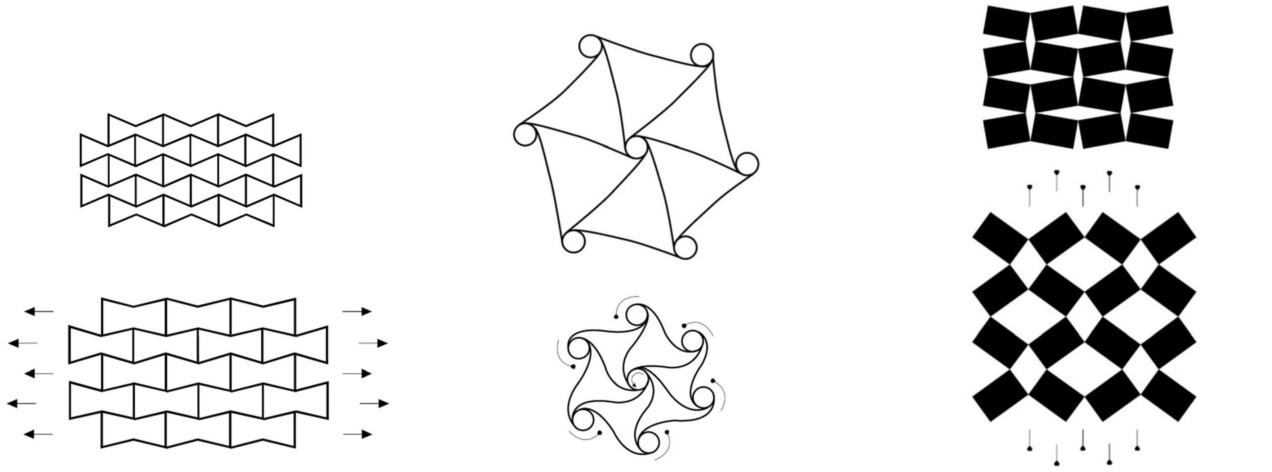

(a) Re-entrant structure (b) Chiral structure (c) Rotating (semi-)rigid structure

Figure 1: Types of auxetic structures [3]

Re-entrant structure (1a) is a type of honeycomb. The difference being the inward directed angle that implies an alignment of the cell ribs when submitted to loads. As seen on Figure 1, a lengthening in one direction decreases the re-entrant angle θ that induces a lengthening in the perpendicular direction [3].

Chiral structure is composed of a cylindrical central unit to which are tangentially attached a defined number of ligaments. Under loads, cylinders rotates and ligaments flex. These structures exhibit a Poisson's ratio close to -1 [3].

Rotating (semi-)rigid structure are composed of rigid squares/rectangles/triangles connected by simple hinges. Under loading, the (semi-)rigid structures rotate at their vertices around the hinges and allow this auxetic behaviour [3].

2.2 Study of Nike patent

In this project, the analysis of the auxetic behaviour is focused on sport applications. An existing patent of an auxetic shoe made by Nike was analysed [2]. The complexity of auxetism was highlighted through this patent. Auxetic sole allows a better shock absorption while taking into account the fact that the foot expands in both lateral and longitudinal direction. Two load cases induce two different behaviours.

Figure 2: Nike auxetic shoe sole [1]

If subjected to vertical compression, as the shoe hits the ground, the triangular void size is reduced as the triangular portions are forced toward the center. If subjected to lateral or longitudinal tension, as the shoe flexes during bending of the foot, the sole expands in both lateral and longitudinal directions due the opposite rotation of the triangular portion, compared to the vertical compression [1].

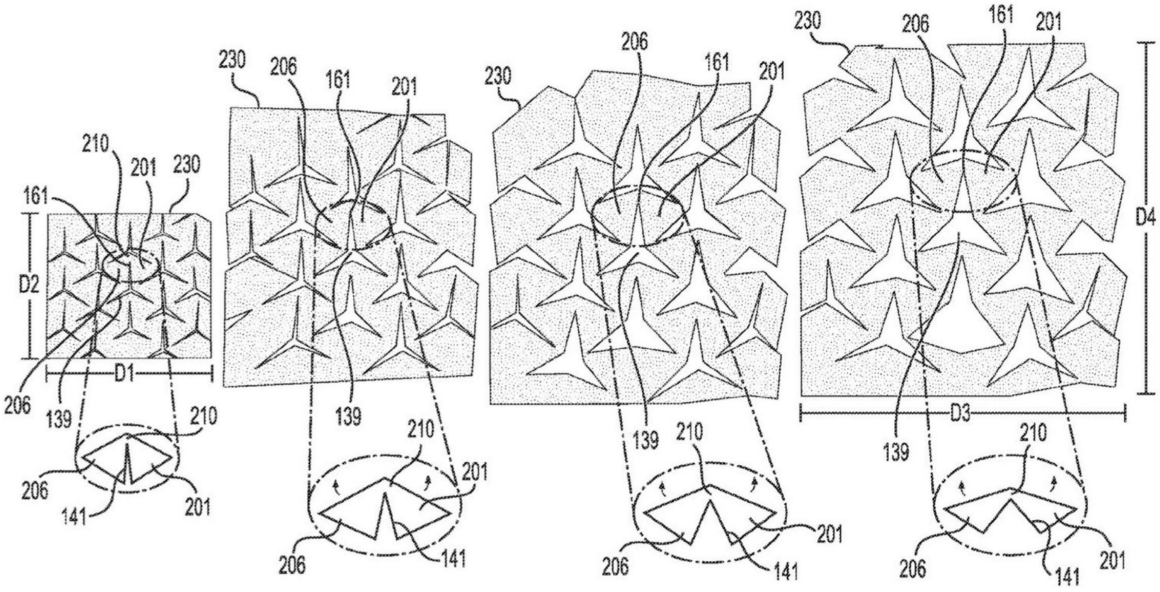

Figure 3: Hinge rotation sequence [2]

The two different behaviours are mostly visible on the bottom plane of the sole. Respectively, triangles rotation when compressed or tensioned implies a closing or an opening of the central star. This change in the sole architecture allows the lengthening or shortening in both transversal and longitudinal directions. On Figure 3, the hinge rotation sequence is presented. On Figure 4, this resulting behaviour is presented in a more precise way.

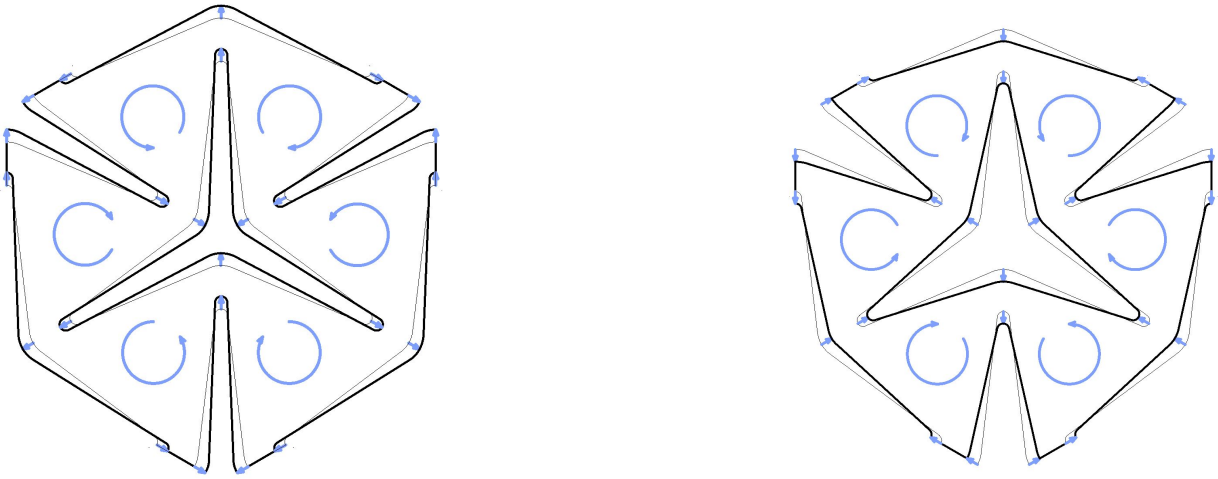

(a) Closing of the central star due to vertical compression

(b) Opening of the central star due to lateral/longitudinal tension

Figure 4: Behaviour of the bottom surface of the sole based on loading conditions

Unlike the opening of the void that is due to an in-plane tensile loading, the closing of the star-shaped void is due to a different mechanism. As we can see on Figure 5 the star closes due to an out-of-plane loading. Unlike auxetic foams which are auxetic due to a nano/micro structure, the shoe sole is auxetic due to a void arrangement; the material in itself has usual properties with a positive Poisson's ratio. Therefore, when subjected to compression, this material will shorten in the load application direction and will expand in the perpendicular direction. By focusing on this lengthening, if the material is filled with voids, they will tend to close. That is what happens to the sole under a compressive load.

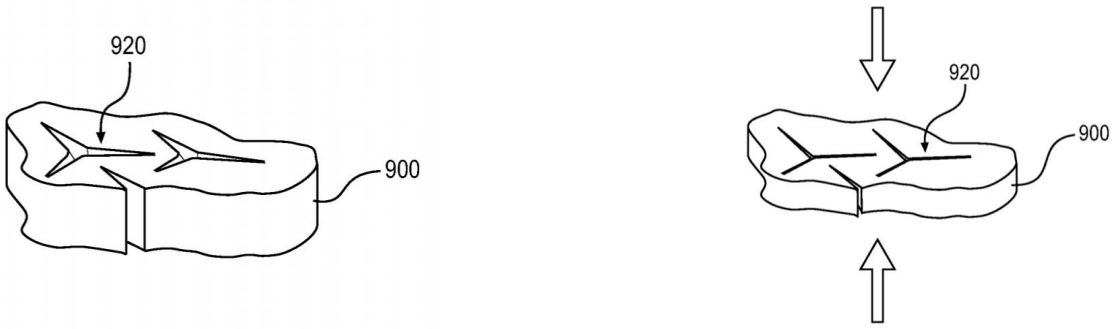

Figure 5: Behaviour of the shoe sole while compressed [2]

In this study, focus is put on the first load case, that is vertical compression. This is a first step to the full understanding of the sole behaviour. Moreover, the closing or opening mechanism of the bottom plane is the same for both load cases and vertical compression is easier to implement, both for simulation and testing.

2.3 Contact and interest in auxetism

Many companies were contacted, especially in the field of grips, regarding the interest that auxetic materials would have in this field since it is still something in development.The answers were positive. Although auxetic grip is not something these companies have ever heard about, it came out that satisfactory grips with these type of materials/structures would interest these companies. A brief contact with the University of Purdue was also very encouraging in the potential auxetism could bring to the sport field.

3 Parametric study

3.1 Auxetic cell modelling

In order to better understand the auxetic structure, tests, either by finite elements or with machines on 3D samples, have to be conducted. It is necessary to model the auxetic element in 3D. The sole auxetic cell is modeled with Fusion 360 software [4]. In addition to the parametric design, it allows a mesh generation and its refinement as well as simulations. These simulations will be performed to better understand the sole auxetic behaviour.

An auxetic cell is made out of an hexagon with a star-shaped void in its middle. The void arrangement generates the rotating (semi-)rigid structure by creating the (semi-)rigid structure attached by hinges. To model the void, two different stars, of different sizes, with 3 arms are created; these will represent the top and bottom part of our void element. A solid connects these two elements placed at a distance that represents the height of the void. This void, still represented by a solid, is then extruded into the hexagon. For a later connection between these auxetic cells, it is also necessary to remove a third of the void on each side of the hexagon, cells overlapping each other. This second extrusion process result is seen on Figure 7. In order to make comparative studies easier between different types of auxetic cells, a parametric representation is chosen. The parameters are defined as following:

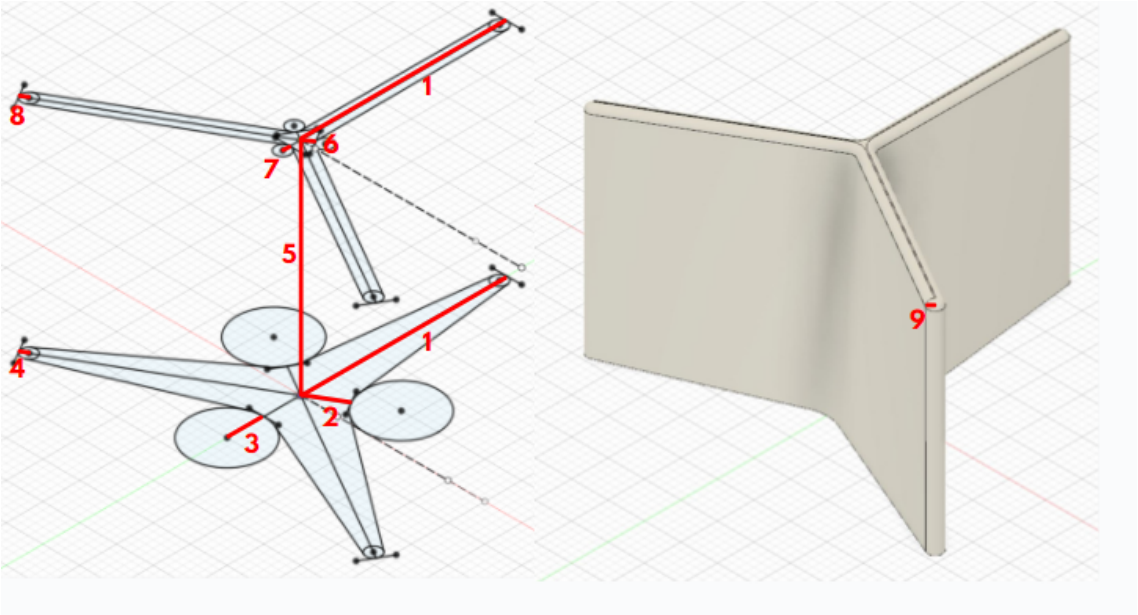

Figure 6: Parametric representation

1. **Arm length :** Length of the arms of the star
2. **Center distance - bottom :** Distance between the center of the bottom star and the tangent point of the circle used to model the internal curvature of the star
3. **Internal radius of curvature - bottom :** Radius of curvature of the internal part of the star
4. **External radius of curvature - bottom :** Radius of curvature of the external part of the star
5. **Void height :** Vertical distance between bottom and top stars

   The same parameters are used to model the top part
6. **Center distance - top**
7. **Internal radius of curvature - top**
8. **External radius of curvature - top**

9. **Fillet top :** Radius of curvature used to round the top part of the void. The use of this parameter will therefore decrease stress concentration in the next steps.

A base auxetic cell is modeled. Its parameters are set as following for a side length of $L_{side,hexagon} = 40[mm]$:

1. **Arm length :** 28 $[mm]$
2. **Center distance - bottom :** 5 $[mm]$
3. **Internal radius of curvature - bottom :** 5 $[mm]$
4. **External radius of curvature - bottom :** 1 $[mm]$
5. **Void height :** 30 $[mm]$
6. **Center distance - top** 1.22 $[mm]$
7. **Internal radius of curvature - top** 1 $[mm]$
8. **External radius of curvature - top** 1 $[mm]$
9. **Fillet top :** 0.92 $[mm]$

The 3D model can be seen at Figure 7.

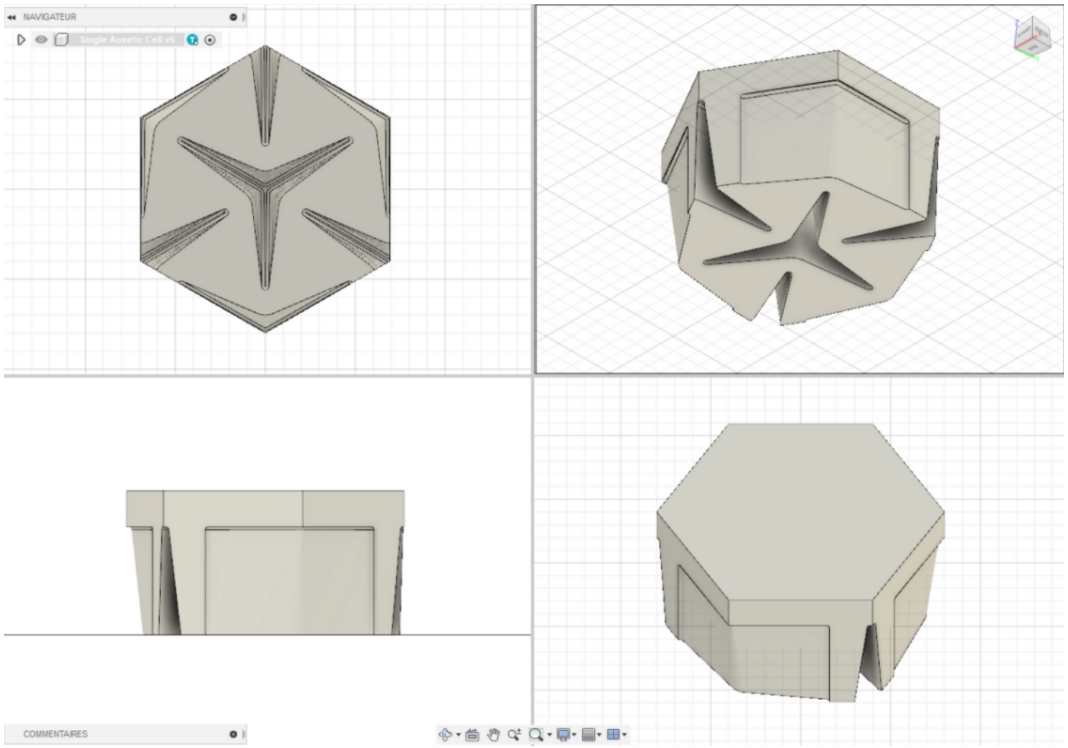

Figure 7: Auxetic cell

As explained before, the particular shape of these cells gives the auxetic behavior. Moreover, they are designed in such a way that they can be combined directly with each other, which will allow us to make more complex models, but above all, it is more complete for the analysis. It will be possible to study the importance of the interaction of the cells. The multiple cell combination is presented on Figure 8.

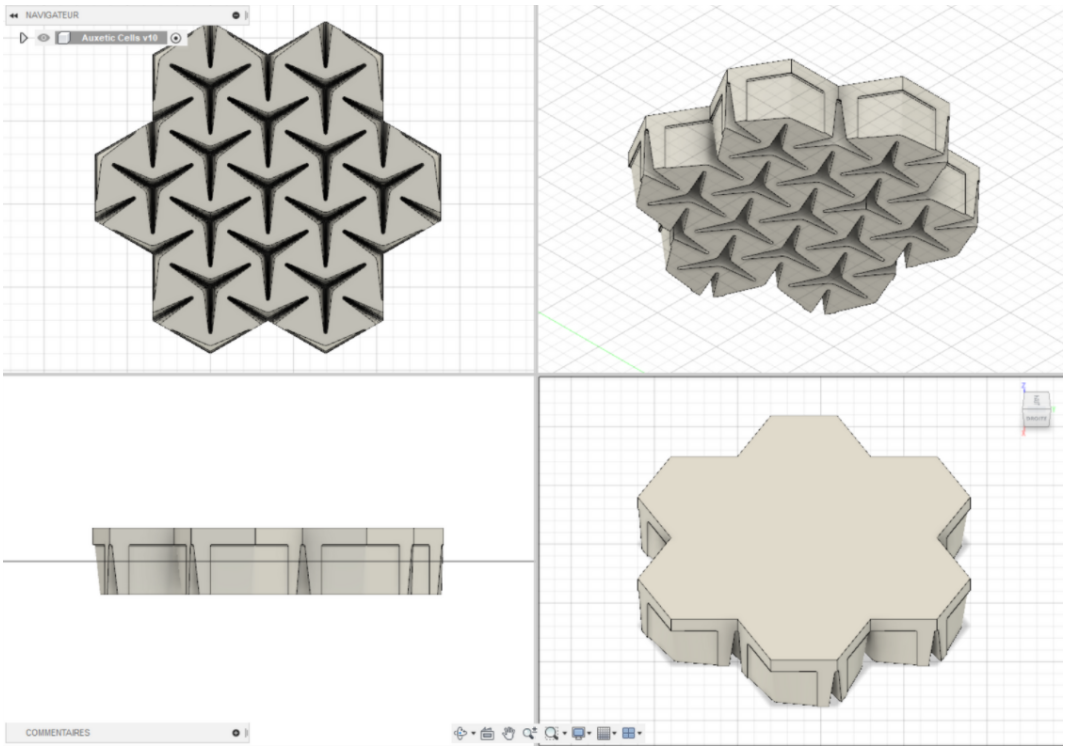

Figure 8: Multiple cells

Both simple and multiple cell model will be studied. However, as a matter of simplification, FEM simulations will only be performed with single auxetic cells. The multiple cell model will be used in real tests. The cells interaction will however be considered even in the case of a single cell, by the application of appropriate boundary conditions.

3.2 Model simulation

3.2.1 Movement constraints

To reduce calculation time, a single auxetic cell is used for FEM simulation. It is possible to reproduce the same behaviour with a single cell as with several ones. However, to get to this result, it is fundamental to correctly set the constraints acting on the cell.

- Side movement constraints

  Auxetic cells are connected to each other thanks to thin material parts acting like hinges and to the plain top part that assembles the rotating triangles: this forms a L-shaped connection on the six sides of the cell. To recreate the effect of surrounding cells, an appropriate movement constraint is applied. Focusing on one side of the cell:

  - Normal movement is prevented by the adjacent cell; a constraint needs to prevent it.
  - Tangential movement is not prevented as the adjacent cell has the same behaviour and will therefore have the same movement; no constraint is needed

  A solution for both of these movements is the application of a "no friction" boundary condition. It prevents an out-of-plane movement while allowing a free in-plane movement along the surface. This constraint is applied to the six L-shaped connections around the cell.

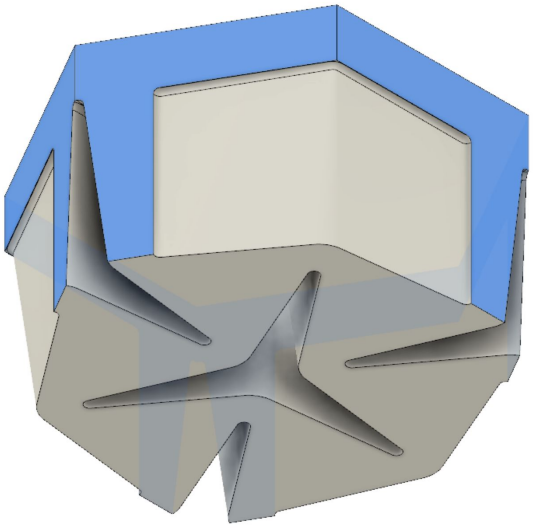

Figure 9: Constraints on the sides of the cell set as "no friction"

- Bottom movement constraint

  Usually, the sole made out of auxetic cells comes directly into contact with the ground. That implies a certain friction between the two surfaces which will mitigate the auxetic effect of the sole. To highlight the desired behaviour in the most unrestrained way, it is therefore necessary to neglect friction. That implies allowing the tangential movement.

  Moreover, normal movement is prevented by the contact on the ground.

  The same way as the side movement constraints, these two bottom movement constraints characteristics are modeled thanks to the no-friction constraint.

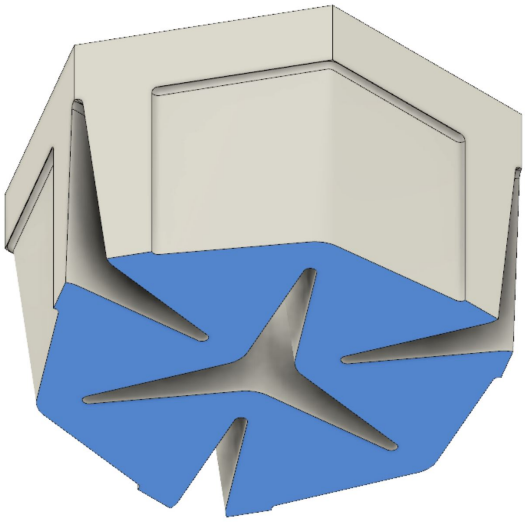

Figure 10: Constraints on the bottom of the cell set as "no friction"

Seven surfaces of the cell with more than three different directions are subjected to the no-friction constraint. Stability of the model is guaranteed.

3.2.2 Type of analysis and load definition

Load is a pressure applied on the top surface of the cell, therefore modelling the force applied by the foot on a portion of a shoe while running.

To reproduce the sole behaviour material is chosen accordingly; silicon rubber is used. Its characteristics are :

$E = 0.003\,[GPa]$
$\nu = 0.49$
$G = 1.007[MPa]$

A linear analysis is performed on the cell subjected to a compressive force. Although big deformations are to be expected, and that an analysis allowing these might be more appropriate, the calculation time is much higher. To characterize the auxetic effect, a parametric study will be made, meaning a high number of simulation have to be performed. That forces the calculation time to be decreased.

The cell deformation is therefore expected to evolve linearly compared to the pressure applied. This load value can be set arbitrarily at 0.3 [MPa].

3.2.3 Meshing of the Auxetic Cell

Meshing is a primordial part in modeling. The more refined the mesh is, the more precise results will be but the longer the calculation time is. For this simulation, we have numerous places were stress concentration is expected, especially at the top part of the star-shaped void. Therefore, the mesh needs to be refined at these critical points. The mesh is directly calculated by Fusion360. Defining parameters used for the mesh are the following:

- Type of element used: T6
- Mean size value of an element based on the model size: 3%
- Minimum size value of an element based on a mean sized element: 20%
- Adaptative refinement of the mesh: 4 iterations, based on Von Mises stresses

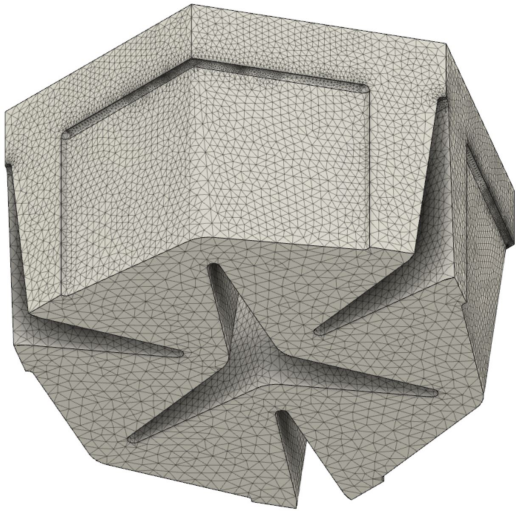

Figure 11: Mesh of the auxetic cell : element sizes are refined at critical points

3.2.4 Auxetic cell behaviour

According to Nike patent [2], the sole exhibits an auxetic behaviour the same way as rotating rigid structures do. The main difference is the vertical change of the void. Indeed, looking at an elevation of the void, the width is not constant and decreases linearly from the bottom part to the top part. The auxetic effect should therefore be the most visible on the bottom surface, with the closing of the star-shaped void under compression. Simulation allows the verification of such statements.

With the movement constraints and the load described in 3.2.1 and in 3.2.2, results are the following:

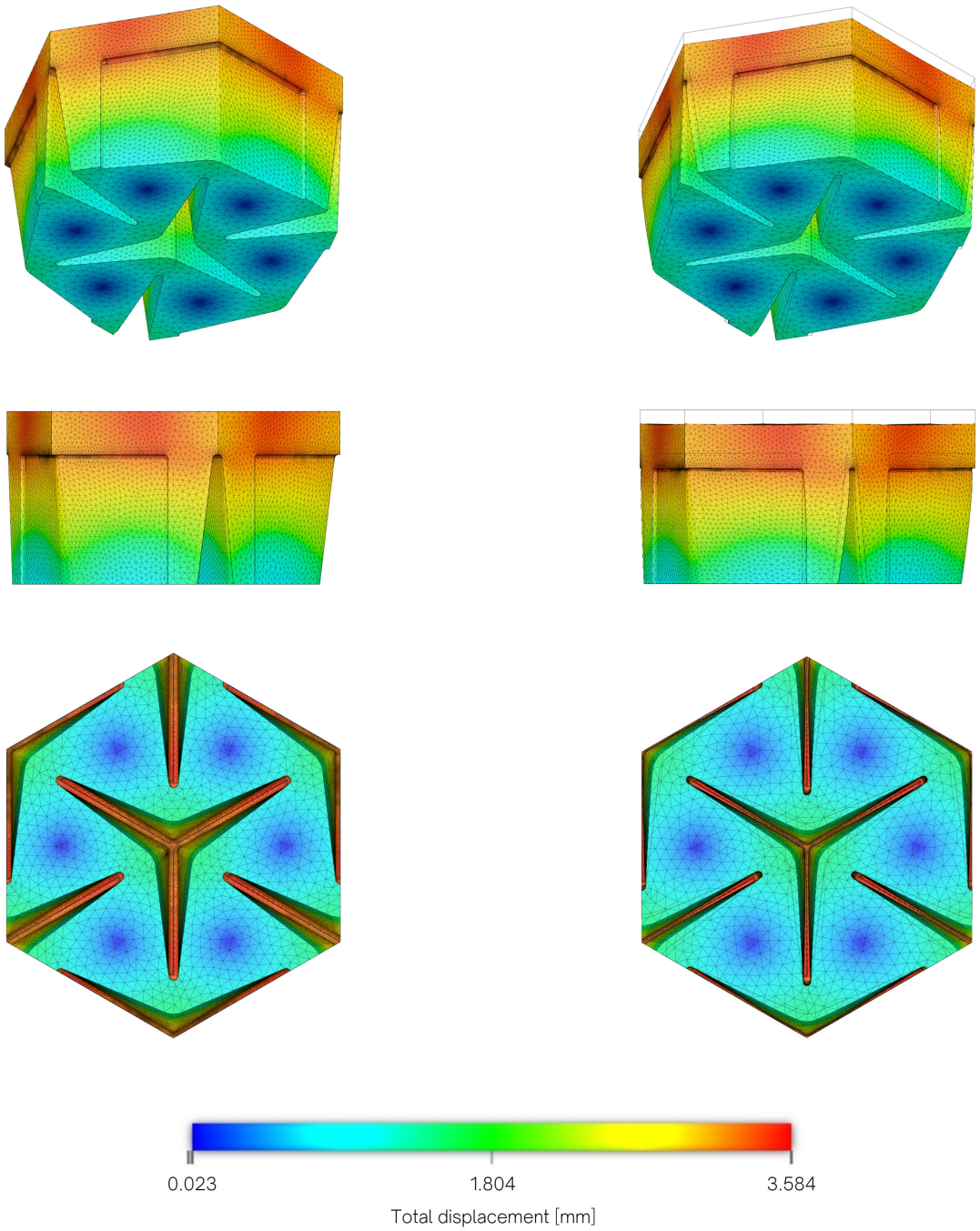

Figure 12: Auxetic behaviour obtained through linear analysis : undeformed model (left) and deformed model 1x (right) - Total displacement

The model exhibits the same behaviour as the one described in the patent. The closing of the star is due to the rotation of the triangular structures around the hinges. Therefore, the model is verified and can be used for further analysis. As for now, the void closing measurement is not obvious. However, to understand the full complexity of this auxetic structure, it is primordial to analyse exhaustively which parameters dictate the deformation of the sole. This will allow the evaluation of the auxetic effect.

4 Measuring the auxetic effect

The next step is therefore the development of a method allowing the measurement of the auxetic effect. For the differents methods, it is assumed that parameters that would be the most impactful on the behaviour are:

- Arm Length : calculation made for 24, 26, 28, 30 and 32 [mm]
- Center Distance - bottom : calculation made for 3, 4, 5, 6, 7 and 8 [mm]
- Void Height : calculation made for 10, 20, 30, 40 and 50 [mm]

4.1 Auxetic behaviour usual measurement

Auxetic materials are easily findable as foams. From polyurethane to epoxy or metallic foams, the structures composing them are on a complex nano/micro scale. It allows the material to exhibit the right behaviour while staying homogeneous. Therefore, the measurement of the auxetic effect is as simple as the calculation of the Poisson's ratio. For a transversal deformation ϵ_{trans} and a longitudinal deformation ϵ_{long}, it is calculated as:

$$\nu_{auxetic} = -\frac{\epsilon_{trans}}{\epsilon_{long}} \tag{1}$$

For re-entrant structures, a macro scale measurement is also possible as the behaviour exhibits itself for a single cell.

For our case, auxetism is not that easily measurable. In fact, the cell is adapted to the sole of a running shoe and can not be analyzed as an homogeneous material. Moreover, a sole cell taken separately deforms as a normal material with the positive Poisson's ratio of the rubber. The desired behaviour is only due to the interaction between the cells. This one cell behaviour is compared to a cell interacting with others and can be seen on figure 13.

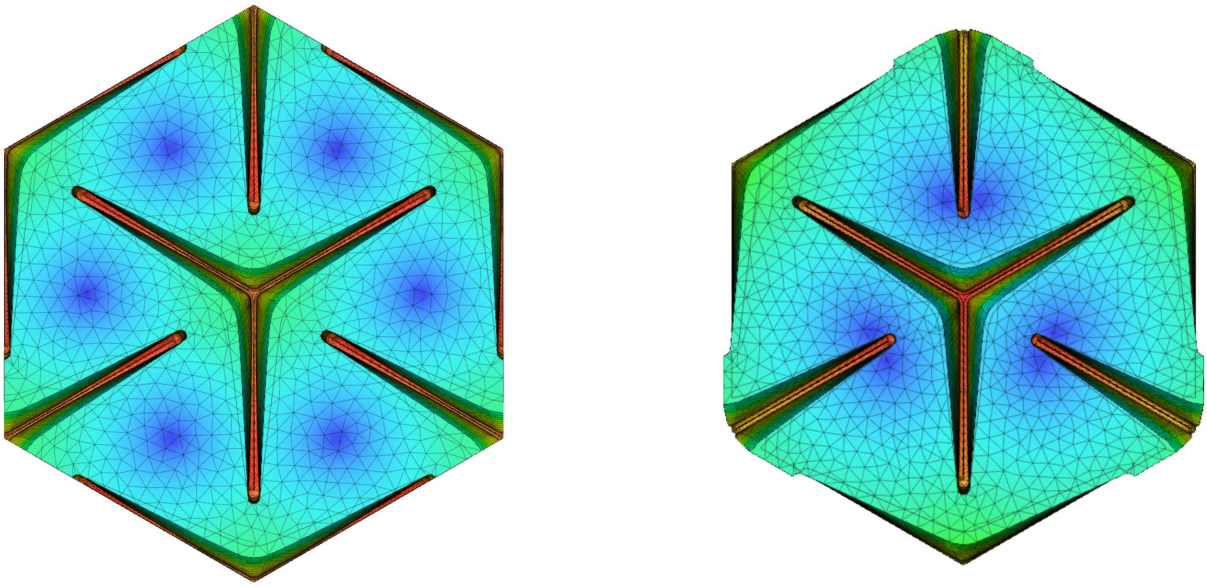

(a) Interacting auxetic cell under compression

(b) Non interacting auxetic cell under compression

Figure 13: Difference between an interacting cell and a non interacting cell

4.2 Calculation methods

As it will be seen in the following section, defining the auxetic behaviour of such cell present a lot of difficulties. For each calculation method, both relative and absolute results are analysed. Relative results are the deformation compared to the potential of deformation; it therefore range between 0, for no closure to -1 for a full closure of

the void. This potential will be defined differently according to each method. Absolute results are deformation normalized on a constant dimension of the cell. This normalization factor is also set differently for each method and does not change when parameters vary. It is also important to note that it is not pertinent to compare the values between the methods as the calculation and the dimension is different. What is interesting to study, are the different trends that results from the methods.

4.2.1 Method I - Linear deformation

Relative changes - ϵ_r vs. ϵ_z

The first method used in order to find a way to measure the auxetic behaviour is based on the classic Poisson's ratio calculation. Calculations are based on the radial deformation ϵ_r and the vertical deformation ϵ_z.

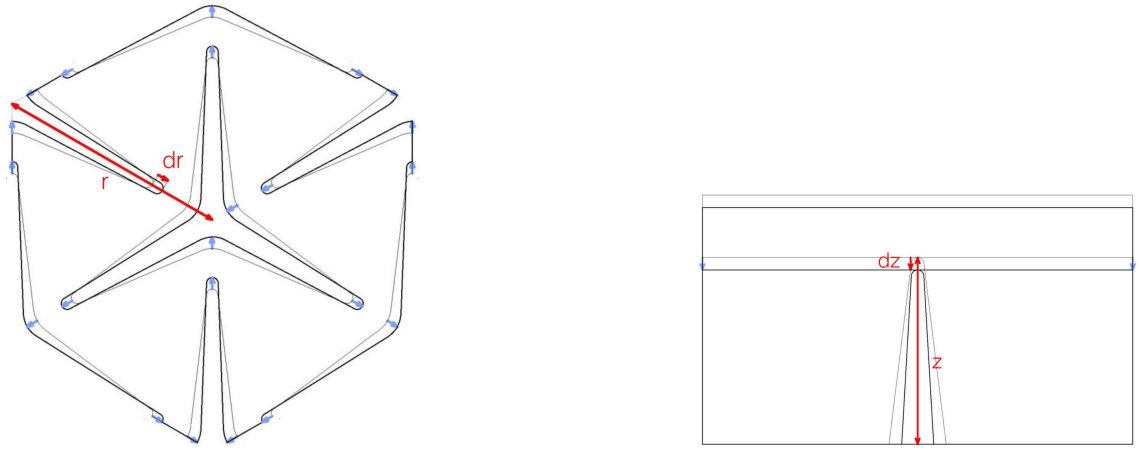

(a) Radial deformation

(b) Vertical deformation

Figure 14: Deformations of the cell taken into account in Method I

- Radial deformation ϵ_r (14a) is the relative closing of the star on the bottom plane. For a side length of the hexagon that also represents the distance between the symmetrical center and a vertex $L_{side,hexagon} = L_{center-vertex} = r$, and for a closing of the star d_r, the deformation is:

$$\epsilon_r = \frac{d_r}{r} \tag{2}$$

- Vertical deformation ϵ_z (14b) is the relative movement in height of the cell. For this calculation, the plain part of the sole is not taken into account as it is just a way to attach the triangular structure together; it does not have an effect on the auxetism. Therefore, for a height of the void $H_{void} = z$, and for a displacement along the vertical axis d_z, the deformation is:

$$\epsilon_z = \frac{d_z}{z} \tag{3}$$

The same way it would be calculated for a Poisson's ratio, the auxetic effect of the method I $AE_{rel,I}$ would then be calculated as:

$$AE_{rel,I} = -\frac{\epsilon_r}{\epsilon_z} \tag{4}$$

Contrary to what has been defined before, the result range of this relative calculation is not limited between 0 and -1. The results of this method will therefore not be fully consistent with the others two methods.

Absolute changes - ϵ_r

Absolute changes of this method are simply the radial deformation ϵ_r., the normalization factor being the center to vertex distance of the hexagon.

$$AE_{abs,I} = -\epsilon_r \tag{5}$$

4.2.2 Method II - Change in surface of the bottom plane

For relative results, the potential of deformation is considered to be the initial void area of the cell. For absolute results, the constant dimension of the cell is the hexagon area (void + material).

Relative changes - change in surface vs. potential of deformation

The second method used is based on the change of area on the bottom surface. As the rotating rigid structures behaviour is easier to define in a 2D plane and since the bottom surface of the sole exhibits the clearest auxetic effect, its area is computed before and after the cell is loaded. The parameters are defined as follows:

- Initial Void area $A_{void,i}$ is the area on the bottom surface of the cell void when the 3D cell is under no solicitation.
- Final Void area $A_{void,f}$ is the area on the bottom surface of the cell void when the 3D cell is loaded.

As Fusion360 does not allow area measurement after the model undergoes an analysis, a deformed model based on d_r and $\dot{z}$ was used to compute the different areas. This deformed model leads to approximations that could be discussed.
Calculations are based on the differences in area:

Change in void area dA_{void} is the difference between the final and the initial cell void area, relative to the initial void area.

$$AE_{rel,II} = dA_{void} = \frac{A_{void,f} - A_{void,i}}{A_{void,i}} \tag{6}$$

Absolute changes - change in surface vs. initial surface of the hexagon

Absolute change of this method is the comparison between the change in surface $A_{void,f} - A_{void,i}$ and the initial hexagon surface $A_{hexagon} = 4157\ [mm^2]$. The normalization parameter does not change in function of the cell parameters.

$$AE_{abs,II} = \frac{A_{void,f} - A_{void,i}}{A_{hexagon}} \tag{7}$$

4.2.3 Method III - Change in volume

For relative results, the potential of deformation is considered to be the initial void volume of the cell. For absolute results, the constant dimension of the cell is the initial volume of the extruded hexagon (void + material).

Relative changes - change in volume vs. potential of deformation

The third method used is based on the change in volume of the cell under a compression load. With the void volume decreasing as the star closes, its relation with the auxetic effect was studied. To measure this change, different parameters are defined:

- Initial Void volume $V_{void,i}$ is the volume of the cell void under no solicitation. It is defined as the volume of the extruded hexagon of height h_{void} to which the material volume is deducted. This volume depends on the parameters defining the cell.
- Final Void volume $V_{void,f}$ is the volume of the cell void under a compression load.

As the software Fusion360 does not allow the user to measure volumes after the model undergoes an analysis, neither it allows to export the mesh, the volumes were calculated based on the radial and vertical displacements, respectively d_r and d_z. As the cell is parametric, it is simple to redefine a new geometry after taking these displacement into account, in order to obtain the volume value. This calculation is therefore subjected to slight model errors. However, it still gives a good approximation.

Calculations are based on the differences in volume:

Change in cell void volume dV_{void} is the difference between the final and the initial cell void volume, relative to the initial void volume.

$$\Delta AE_{rel,III} = dV_{void} = \frac{V_{void,f} - V_{void,i}}{V_{void,i}} \tag{8}$$

Absolute changes - change in volume vs. initial volume of the extruded hexagon

Absolute change of this method is the comparison between the change in volume $V_{void,f} - V_{void,i}$ and the initial extruded hexagon volume V_{eh}. It is important to note that the height of the extrusion is of h_{void} as the top plain part of the cell does not exhibit an auxetic behaviour. Therefore, normalization factor V_{eh} is constant for "Center Distance - bottom" and "Arm Length" parameters as h_{void} is kept constant at 30 $[mm]$. However, this factor increases as void height and V_{eh} increase.

$$AE_{abs,III} = \frac{V_{void,f} - V_{void,i}}{V_{eh}} \tag{9}$$

4.3 Results

4.3.1 Method I - Deformation ϵ_r and ϵ_z

The basic auxetic cell with the parameters indicated in 3.1 have the following characteristics:

- Radial deformation $\epsilon_r = 0.039\ [mm]$
- Vertical deformation $\epsilon_z = 0.114\ [mm]$
- Relative Auxetic Effect I $AE_{rel,I} = -0.340$
- Absolute Auxetic Effect I $AE_{abs,I} = -0.039$

When a parameter is changed, other parameters are kept constant at their base value, defined in Section 3.1. The results for the range of parameters studied are the following one :

Parameter	ϵ_r	ϵ_z	$AE_{rel,I}$	$AE_{abs,I}$
Center Distance - bottom $[mm]$				
3	0.036	0.105	**-0.346**	-0.036
4	0.037	0.109	-0.341	-0.037
5	0.038	0.114	-0.337	-0.038
6	0.040	0.119	-0.337	-0.040
7	0.042	0.124	-0.334	-0.042
8	0.044	0.130	-0.334	**-0.044**
Void height $[mm]$				
10	0.027	0.107	-0.256	-0.027
20	0.037	0.110	-0.333	-0.037
30	0.039	0.114	-0.340	-0.039
40	0.040	0.116	-0.340	-0.040
50	0.040	0.117	**-0.340**	**-0.040**
Arm Length [mm]				
24	0.038	0.106	**-0.361**	-0.038
26	0.039	0.111	-0.349	-0.039
28	0.039	0.114	-0.342	-0.039
30	0.040	0.117	-0.337	-0.040
32	0.040	0.121	-0.331	**-0.040**

Table 1: Relative and absolute auxetic effect according to Method I

The relative and absolute auxetic effect are plotted with respect to the three different parameters studied. Differences between the two calculation modes can be analysed as well as the influence of each parameter on the cell behaviour.

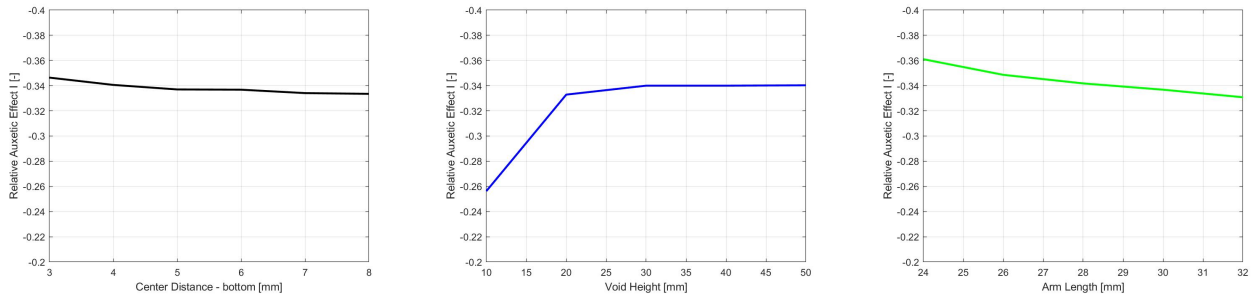

(a) Center Distance - bottom (b) Void Height (c) Arm Length

Figure 15: Relative Auxetic Effect of the different parameters - Method I

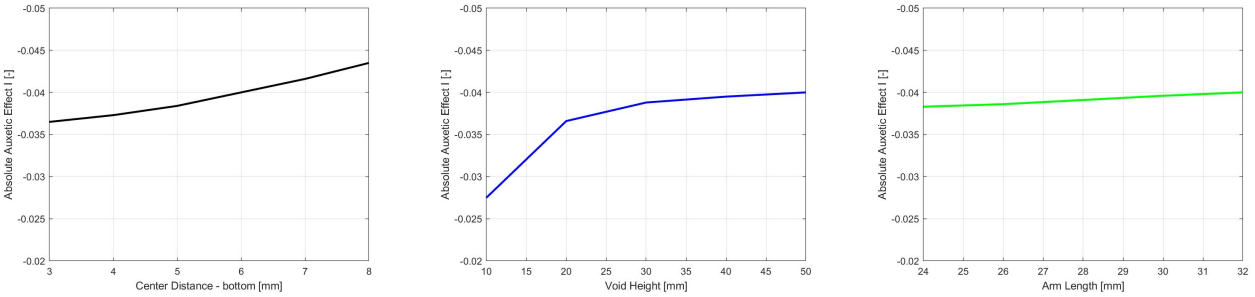

(a) Center Distance - bottom (b) Void Height (c) Arm Length

Figure 16: Absolute Auxetic Effect of the different parameters - Method I

According to the graphs, the relative and absolute methods seem to show opposite trends for both "center distance" and "arm length" parameters. In fact, in the relative calculation, there is a dependency of ϵ_z on

the cell shape, that changes according to the different parameters. That could slightly alter the results. For exemple, by comparing the relative and absolute results of the "center distance - bottom" parameter, there is respectively a decrease and an increase in the auxetic effect as the star void opens. With a bigger void, vertical deformation increases and therefore, the result of $AE_{rel,I}$ (4) decreases. For the absolute calculation, we observe a bigger auxetic effect when the distance to the center increases; for relative calculation, this is counteracted by the dependency on vertical deformation.

By taking that into account, it seems, that the absolute effect is more representative. Therefore:

- A higher distance to the center increases the star-closing effect from -0.036 to -0.044.
- An increasing void height increases this star-closing effect until it reaches a plateau of ~ -0.04 at a height value of 30 $[mm]$.
- Arm length seems to have little to no effect on the auxetic effect as the value ranges between -0.038 and -0.040 respectively for an arm length of 24 $[mm]$ and 32 $[mm]$.

4.3.2 Method II - Change in surface of the bottom plane

The basic auxetic cell with the parameters indicated in 3.1 have the following characteristics:

- Initial void area $A_{void,i} = 1203\ [mm^2]$
- Final void area $A_{void,f} = 901\ [mm^2]$
- Change in void area $\Delta A_{void} = -302\ [mm^2]$
- Relative change in void area on the bottom surface $AE_{rel,II} = -0.252$
- Absolute change in void area on the bottom surface $AE_{rel,II} = -0.073$

The results for the range of parameters studied are the following one :

Parameter	$A_{void,i}\ [mm^2]$	$A_{void,f}\ [mm^2]$	$\Delta A_{void}\ [mm^2]$	$AE_{rel,II}$	$AE_{abs,II}$
Center Distance - bottom $[mm]$					
3	751	440	-311	**-0.414**	**-0.075**
4	978	673	-305	-0.311	-0.073
5	1203	904	-299	-0.249	-0.072
6	1427	1128	-299	-0.210	-0.072
7	1650	1354	-296	-0.179	-0.071
8	1871	1576	-295	-0.158	-0.071
Void height $[mm]$					
10	1203	992	-211	-0.175	-0.051
20	1203	918	-285	-0.237	-0.068
30	1203	900	-303	-0.252	-0.073
40	1203	893	-310	-0.257	-0.074
50	1203	889	-314	**-0.261**	**-0.075**
Arm Length [mm]					
24	1034	784	-250	-0.242	-0.060
26	1119	842	-277	-0.247	-0.066
28	1203	898	-305	-0.254	-0.073
30	1287	953	-335	-0.260	-0.080
32	1372	1007	-364	**-0.266**	**-0.087**

Table 2: Relative and absolute auxetic effect according to Method II

The relative and absolute auxetic effect are plotted with respect to the three different parameters studied.

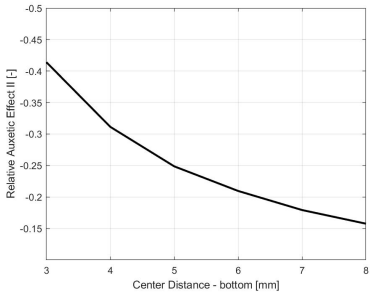

(a) Center Distance - bottom

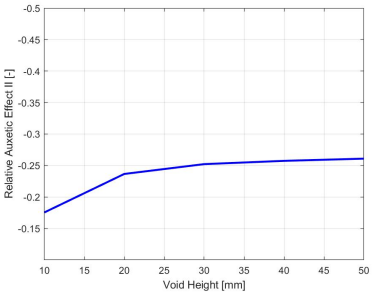

(b) Void Height

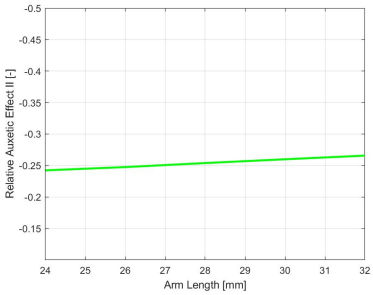

(c) Arm Length

Figure 17: Relative Auxetic Effect of the different parameters - Method II

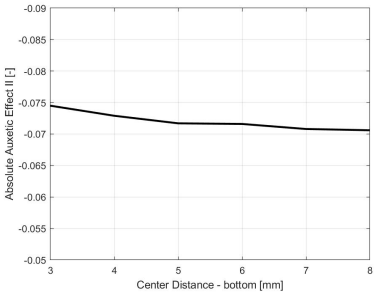

(a) Center Distance - bottom

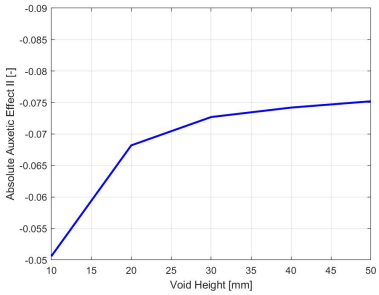

(b) Void Height

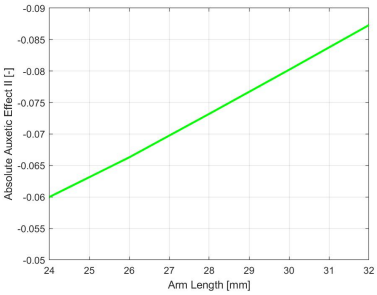

(c) Arm Length

Figure 18: Absolute Auxetic Effect of the different parameters - Method II

According to the graphs, the relative and absolute methods show roughly similar results for the three parameters. Relative calculation (6) need to be put in perspective with a heterogeneity effect. Higher initial void, for a roughly similar ΔA_{void} means that there is an important dependency of the relative results on the initial void area. For example, by comparing the relative and absolute results of the "arm length" parameter, there is respectively a slight ((17)) and a strong increase (18) in the auxetic effect, as the arm of the star void lengthens. The lenghtening of the arm induce a bigger void area and for a roughly similar ΔA_{void}, the result of $AE_{rel,II}$ (6) decreases, which has a direct impact on the trend's intensity.

By taking that into account, it seems, that the absolute effect is more representative. Therefore:

- A higher distance to the center decreases the star-closing effect very slightly, which is in contradiction with Method I.
- An increasing void height increases this star-closing effect until it reaches a plateau of ~ -0.073 at a height value of 30 $[mm]$ accordingly to the results of method I.
- Arm length seems to have an important effect on the auxetism as the value increase from -0.060 to -0.087 respectively for an arm length of 24 $[mm]$ and 32 $[mm]$.

4.3.3 Method III - Change in volume

The basic auxetic cell with the parameters indicated in 3.1 have the following characteristics:

- Initial hexagon volume $V_{hexagon,i} = 124710\ [mm^3]$
- Initial void volume $V_{void,i} = 24494\ [mm^3]$
- Final void volume $V_{void,f} = 17819\ [mm^3]$
- Change in void volume $\Delta V_{void} = -6675\ [mm^3]$
- Relative change in void volume $AE_{rel,III} = -0.272$

- Absolute change in void volume $AE_{abs,III} = -0.053$

The results for the range of parameters studied are the following one :

Parameter	$V_{hexagon,i}$ $[mm^3]$	$V_{void,i}$ $[mm^3]$	$V_{void,f}$ $[mm^3]$	ΔV_{void} $[mm^3]$	$AE_{rel,III}$	$AE_{abs,III}$
Center Distance - bottom $[mm]$						
3	124710	18077	12356	-5721	**-0.316**	-0.046
4	124710	21263	15196	-6067	-0.285	-0.049
5	124710	24491	17825	-6666	-0.272	-0.053
6	124710	27724	20500	-7224	-0.261	-0.058
7	124710	30870	23093	-7777	-0.252	-0.062
8	124710	34110	25672	-8437	-0.247	**-0.068**
Void height $[mm]$						
10	41570	8093	6354	-1739	-0.215	-0.042
20	83140	16244	12089	-4155	-0.256	-0.050
30	124710	24496	17832	-6664	-0.272	-0.053
40	166280	32730	23604	-9126	-0.279	-0.055
50	207850	40950	29403	-11547	**-0.282**	**-0.056**
Arm Length [mm]						
24	124710	21006	15543	-5463	-0.260	-0.044
26	124710	22722	16687	-6035	-0.266	-0.048
28	124710	24496	17799	-6697	-0.273	-0.054
30	124710	26277	18928	-7349	-0.280	-0.059
32	124710	27986	20019	-7967	**-0.285**	**-0.064**

Table 3: Relative and absolute auxetic effect according to Method III

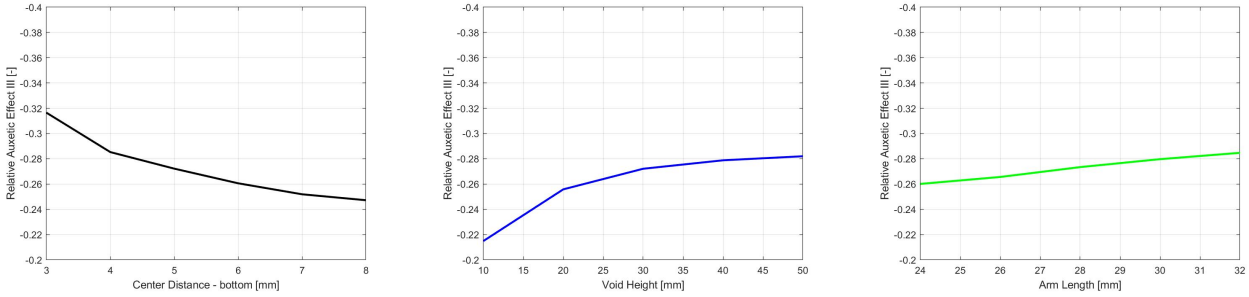

(a) Center Distance - bottom (b) Void Height (c) Arm Length

Figure 19: Relative Auxetic Effect of the different parameters - Method III

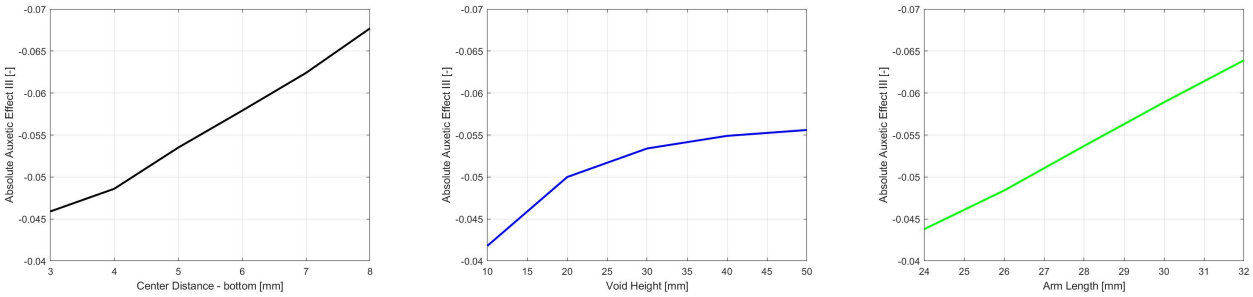

(a) Center Distance - bottom (b) Void Height (c) Arm Length

Figure 20: Absolute Auxetic Effect of the different parameters - Method III

According to the graphs, the relative and absolute methods show similar trends for "void height" and "arm length" parameter. For the "center distance - bottom" parameter, the trends are opposites. Once again, relative

calculation (8) need to be put in perspective with a heterogeneity effect. When varying the parameters, initial void volume $V_{void,i}$ evolves faster than ΔV_{void}. By comparing the relative and absolute opposite results of the "center distance - bottom" parameter, there is respectively a decrease and an increase in the auxetic effect as the distance to the center increases. From $3\,[mm]$ to $8\,[mm]$ of center distance, with a void volume that ranges between $18077\,[mm^3]$ and $34110\,[mm^3]$ and with a ΔA_{void} that ranges between $-5721\,[mm^3]$ and $-8437\,[mm^3]$, the size effect is particularly important and explains the opposites trends

By taking that into account, once again, it seems that the absolute effect is more representative. Therefore:

- A higher distance to the center increases the star-closing effect. This result is in agreement with Method I that showed a slight increase but in contradiction with Method II.
- An increasing void height improves this star-closing effect until it reaches a plateau of ~ -0.055 at a height value of $30 - 40\,[mm]$. This result is in agreement with both previous methods
- Arm length seems to have an important effect on the auxetism as the value increase from -0.044 to -0.064 respectively for an arm length of $24\,[mm]$ and $32\,[mm]$. This result is in agreement with both previous methods although Method I only showed a slight increase.

4.4 Interpretation of the results

As seen with the three different methods, this sole auxetic cell does not allow a simple Poisson's ratio calculation. Determination of the auxetic effect needs to be adapted to the cell heterogeneity. Three methods were tested and both relative and absolute results were studied. However, relative results are difficult to interpret as their calculation is based on varying void size. Absolute results describe the cell behaviour in a more reliable way but the results might be too simple; further investigations are necessary. Final trends of the star-closing effect depend on the different parameters values and are summarized below.

- **Center Distance - bottom**

  For an increasing distance to the center, there is a slight increase in the auxetic effect according to method I, a slight decrease according to method II and a sharp increase in method III. These trends tend to complicate the interpretation but it would seem that an increasing distance to the center would increase the star-closing effect. The optimum value is not found, as there is still a rise at $8\,[mm]$ of opening. However, as the void opens, the initial tri-armed star changes into a triangle. At one point, the (semi-)rigid auxetic structure would therefore disappear as well as the auxetic effect. It is also important to note that as the distance to the center increases, the arm length should decrease. Otherwise, hinges to which each triangle is connected would disappear.

- **Void Height**

  For an increasing void height value, the three methods show similar result, both in relative and absolute calculations. Star-closing effect is constantly increasing but reaches an asymptot at a height value around 30 to $40\,[mm]$. By normalizing this void height by the side length of the hexagon, the optimum void height ratio is reached at:

  $$VH_{opt,min} = \frac{VH}{L_{side,hexagon}} \cong 0.875 \tag{10}$$

  Higher void heights increase the value only very slightly and is therefore not very interesting.

- **Arm Length**

  For an increasing arm length value, the three methods show similar trends although method I shows only a slight increase. Star-closing effect increases and the optimum value is not yet found at $ArmLength = AL = 32\,[mm]$. However, arm length has a direct impact on the hinge width. If the value is too high, the hinge disappears as well as the auxetic effect. Therefore, with $CenterDistance = CD$

  $$w_{hinge} = L_{center-vertex} - AL - CD \geq 0 \tag{11}$$

  Arm Length optimum should be a compromise between the auxetic effect and the stress concentration.

It would then be interesting to study the optimum auxetic cell by optimizing these three parameters. it seems that a void height of $30\,[mm]$, a void opening of $CD = 8\,[mm]$ and an arm length of $AL = 32\,[mm]$ would give that optimal effect. However, as said earlier in (11), the two values of void opening and arm length are not

compatible as the hinge width $w_{hinge} = L_{center-vertex} - AL - CD = 40 - 32 - 8 = 0\,[mm]$. No auxetic effect would be observed. As the parametric study was bounded by the condition of a positive but optimized hinge width, the two optimal cells, with respectively high value of void opening and of arm length, have already been studied. This study is also made from the basic cell parameters defined in 3.1; when a parameter is increased, the other one stays at its basic value. These two optimized cells have the following CD/VH/AL (Center distance [mm] / Void height [mm] / Arm length [mm]) properties:

- "Center Distance - bottom" parameter optimized : 8/30/28
- "Arm Length" parameter optimized : 5/30/32

Auxetic Cell	$AE_{rel,I}$	$AE_{rel,II}$	$AE_{rel,III}$	$AE_{abs,I}$	$AE_{abs,II}$	$AE_{abs,III}$
8/30/28	**-0.334**	-0.158	-0.247	**-0.044**	-0.071	**-0.068**
5/30/32	-0.331	**-0.266**	**-0.285**	-0.040	**-0.087**	-0.064

Table 4: Comparison in results for both cell with optimized parameters

By looking at the table 4, the results are inconclusive. It is not possible to determine which parameter has the biggest impact on the auxetism. In a further study, by setting a minimal hinge width w_{hinge}, arm length and void opening should be varied accordingly to optimize the auxetic effect.

5 3D printing

In order to perform tests, it was necessary to make samples. In that intent, 3D molds were modeled on Fusion360.

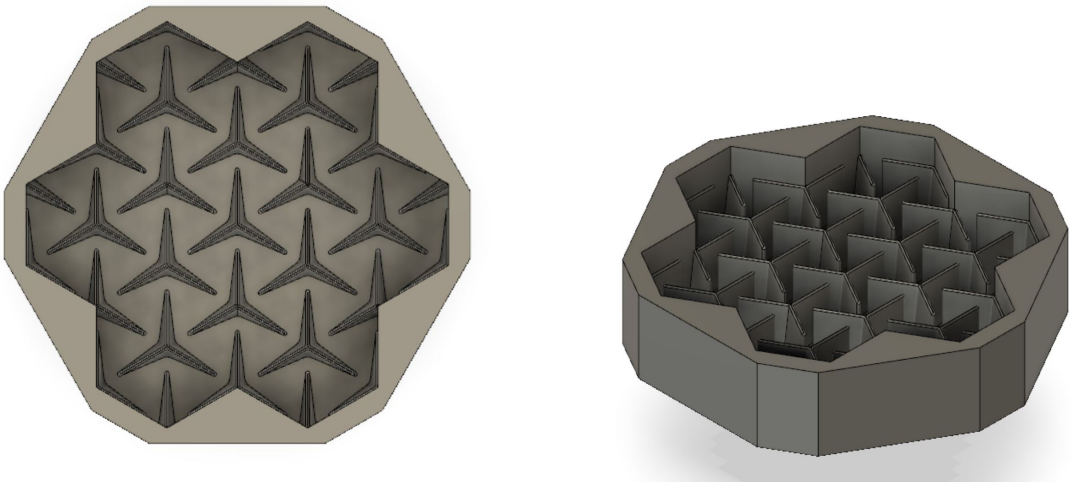

Figure 21: Mold modeled on Fusion360

This first mold was 3D printed on a filament printer as the cell size magnitude was in centimeters and therefore the filament precision of 0.4 $[mm]$ was acceptable. Sample transversal length is $l_{sample} = 10.5\,[cm]$ and its void height is $h_{v,sample} = 1.5\,[cm]$.

An auxetic band mold was also modeled. In fact, in future studies, auxetic band with this type of rotating semi-rigid structure pattern could find different uses. As an exemple, it could be used as overgrips for tennis rackets or as the rubber part of table tennis rackets.

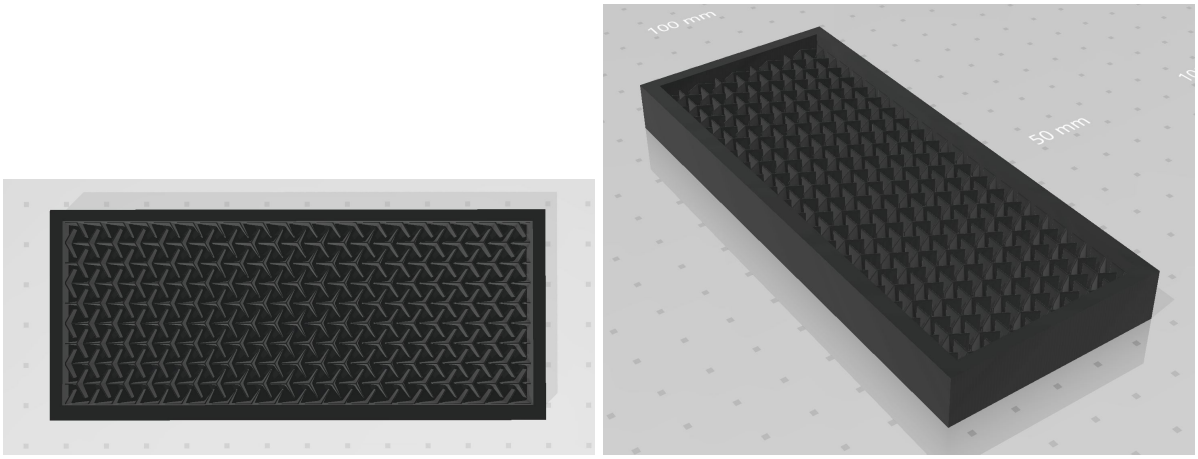

Figure 22: Band mold model

This second mold was 3D printed on a resin printer as the cell size magnitude was in millimeter and therefore the filament precision was not acceptable. Sample length is of $l_{sample} = 10.64\,[cm]$, width is $w_{sample} = 4.18\,[cm]$ and its void height is of $h_{v,sample} = 3.5\,[mm]$.

The next step was the casting of two types of polymer in the 3D printed mold. Two types of silicone were used, with different hardness.

Elite Double 8 (pink-colored) [5]

- Elastic recovery : 99.95%

- Hardness (Shore A) : 8
- Load at break : 2 $[N/mm^2]$
- Elongation at break : 380%
- Tear Resistance : 2.5 $[N/mm^2]$

Elite Double 32 (green-colored) [5]

- Elastic recovery : 99.95%
- Hardness (Shore A) : 32
- Load at break : 2.5 $[N/mm^2]$
- Elongation at break : 350%
- Tear Resistance : 5 $[N/mm^2]$

The obtained samples are the following :

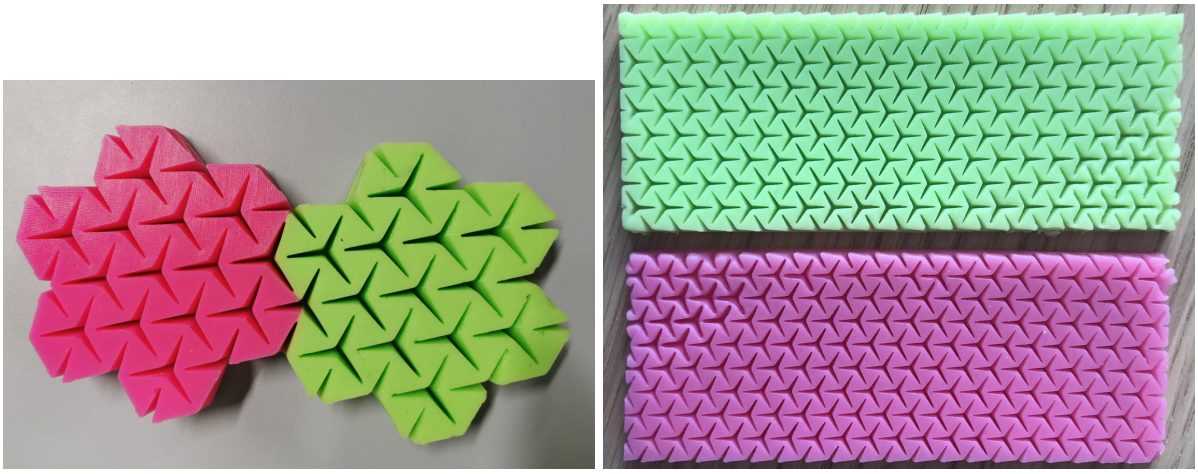

Figure 23: Samples made out of the two molds and the two polymers

Tennis table prototypes were also made.

Figure 24: Tennis table racket prototypes made out of the auxetic bands samples of the two polymers

6 Experimental investigation of friction coefficient

6.1 Deformation under compression load

After modeling the auxetic cell, performing finite element studies and making 3D samples, it was necessary to perform various basic tests to study the properties that these auxetic cells can offer in practice. First of all, it is interesting to study if the desired behavior, i.e. a closing of the stars takes place under a compression load. For this, a simple experiment is done, where the elements are placed on a transparent glass previously lubricated. A metal plate is placed on the top part of the sample to distribute the applied force as uniformly as possible. The assembly can be seen in figure 25. The next step is to load the element progressively, with a manual machine, as it was interesting in a first place to check the behavior rather than having precise values. Thanks to a camera placed underneath the glass sheet, it is possible to visualize the progressive evolution of the deformation and in particular the closing of the stars.

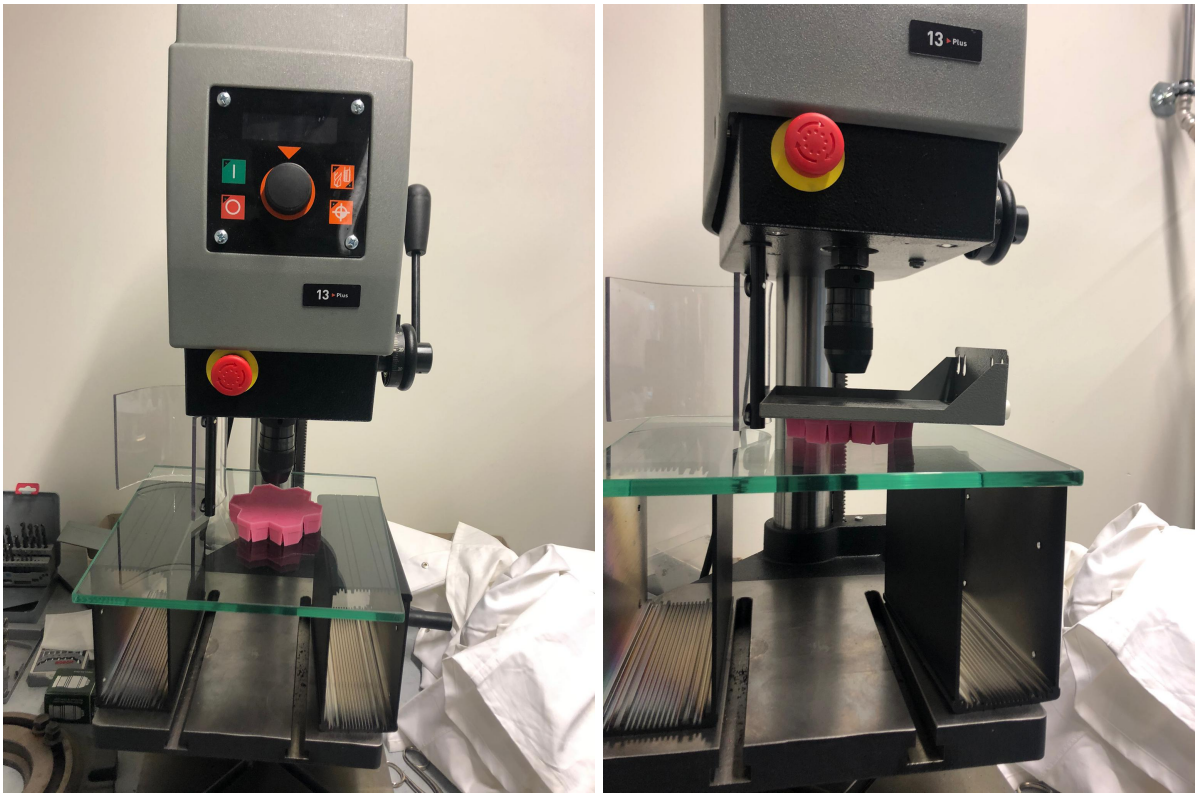

Figure 25: Set up for behavior test under compression load

In figure 26, it is possible to see the evolution of the displacements when compression is applied. Focus should be put on the central star as side cells have free edges and reproduce the effect seen in Figure 13a. The stars close little by little, which shows that the desired behavior is achieved. This also suggests that the sole grip can be increased when the applied force is large enough to activate the auxetism.

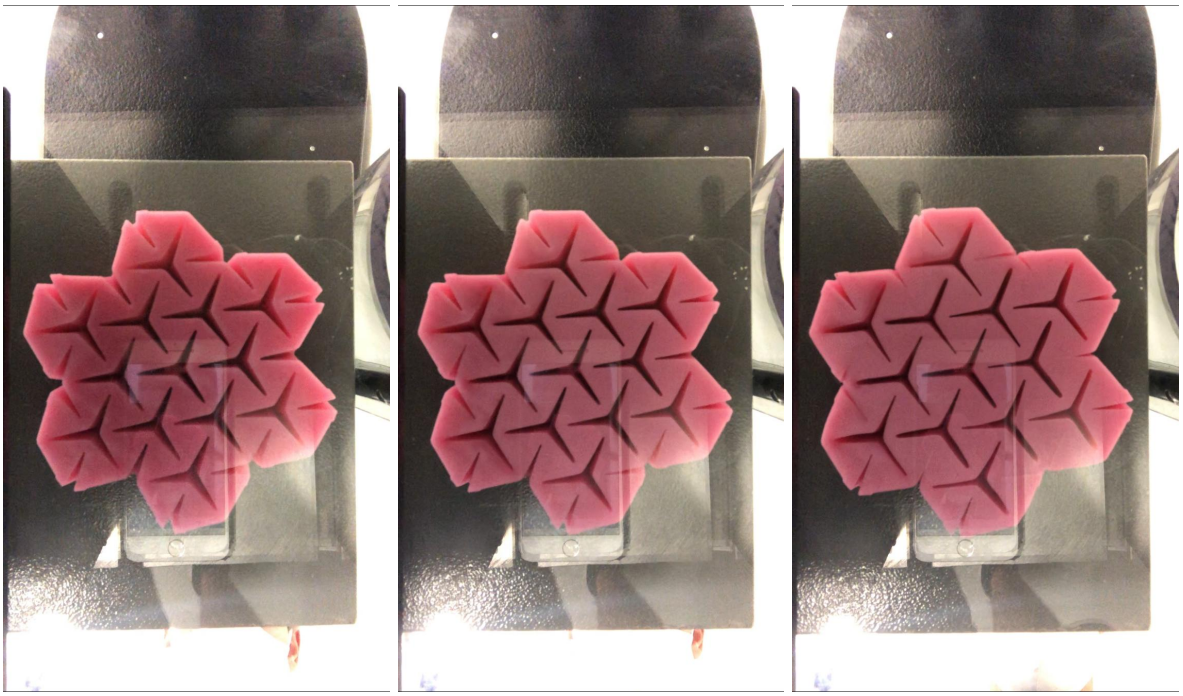

Figure 26: Evolution under compressive load

In order to see if this increase in grip is real, tests on smooth and rough surfaces are performed, to measure an approximate friction coefficient under different normal loads.

6.2 A first foray: Da Vinci friction experiment

At first, a simple test is carried out, to determine the frictional properties of the studied auxetic sample. A rough 3D printed surface that was realized thanks to the python library Tamaas [6] is used. This surface is visible in figure 27.

Figure 27: Rough surface with Tamaas and 3D printing

For the smooth surface, any flat surface is suitable, In this case, a library shelf was used. To uniformly apply the different stresses, a more rigid mold was fitted around the top part of the auxetic sample to which a string is attached. It was then necessary to test, for various normal loads on the mold, the tangential forces necessary to have a first displacement of the sample.

Figure 28: Simple friction test set-up

Note : A surface tilt angle was applied to initiate a displacement with less weights. It is therefore necessary to decompose the different forces in the normal and tangiental components.

The following equations will be used,

$$N = (W_{pp} + W_{weights-top}) \cdot \cos\alpha \tag{12}$$

$$T = (W_{pp} + W_{weights-top}) \cdot \sin\alpha + W_{weights-bottom} \tag{13}$$

with W_{pp} the weight of the elements and the mold ($W_{pp} = 200\,[g]$), $W_{weights-top}$ the weight applied on the mold and $W_{weights-bottom}$ the weight creating the tangential force. Moreover, $\alpha = 16.11°$.

Relationship between normal and tangential force using the friction coefficient is expressed as follows:

$$T = \mu \cdot N \rightarrow \mu = \frac{T}{N} \tag{14}$$

μ is the static friction coefficient corresponding to the curve slope linking N in abscissa and T in ordinate.

Problems in the simple tests soon became apparent. First of all, it was not possible to apply normal forces that were large enough to observe any auxetic effect. This greatly diminished the interest in determining the coefficient of friction since it depends mainly on the materials used. When testing the sample on a rough surface, a tilting phenomenon appeared, giving erroneous results since no displacement along the rough surface took place. This is due to the fact that, with the rough surface, the tangential forces before the first displacement are increased. Therefore, as the force with the string is applied on the upper rear part of the mould, the tilting stability is exceeded before the sliding stability.

6.3 Determine friction with a direct shear device

6.3.1 Preamble to the experiment

It was then necessary to think of a solution to carry out tests in a more correct way, that would allow to obtain more satisfactory results. With the help of Marie Violay, her laboratory, and in particular Laurent Gastaldo, it

was possible to carry out a friction test in the rock mechanics laboratory. This would allow, with the help of a specialized machine, to measure the static and dynamic friction coefficients under different normal loads.

The first critical point is related to the maximum size of the elements that the machine can test. Large auxetic cells do not fit in the boxes used for the machine and are therefore not easily testable. A smaller mold was designed and smaller samples were casted. A rough and a flat surface were also 3D printed with the resin printer.
With smaller samples, the contact surface is smaller and therefore, the compression force applied had to be lower than the previous test. However, this machine would allow more precise results.

6.3.2 Description of the experiment

Operating the machine is fairly simple. On two distinct boxes, the flat/rough surface on which the test will be carried out and the sample to be tested are fixed. Plaster is added in order to avoid any unwanted internal displacement which would disturb the experiment. The boxes are presented on Figure 29.

Figure 29: Preparation of the boxes for experiment

Once the plaster is dry, the boxes are ready to be used. Machine is shown in Figure 30.
The box containing the base surface is placed and locked into the machine so that it is connected to the bottom tray. The upper box containing the sample is placed on top and attached to the fixed part of the machine, so that no movement is possible. Then, weights can be placed at the front of the machine. Thanks to a lever arm, the weights placed at this level will induce a force ten times greater.
At this point, a normal force is applied and the experiment can begin. A horizontal displacement at constant speed is then applied to the lower box, while the upper box remains stationary. The tangential force at the upper box is then measured, which allows to determine maximum tangential force at the first displacement for the static friction coefficient. This also allows to determine the tangential force after the occurrence of the first movement between the sample and the surface. This corresponds to the tangential force for the dynamic coefficient.
Different normal forces are tested to obtain a normal force-tangential force curve. Thus see the evolution of the friction coefficient, if any, in relation with the normal force.

Figure 30: Shear machine

6.3.3 Problems encountered in the test set-up

Carrying out experiments revealed numerous problems. Solutions need to be found to obtain the most precise results possible, despite the difficulties encountered.
The first problem was related to the fact that this machine is used for rocks characterization. The loads applied are therefore really big and the weight of the boxes show on figure (29) has almost no influence on the results. However, since smaller samples had to be made to fit within the size limits of the boxes, a much smaller normal load directly activated the auxetic behavior of the sample. In this case, the weight of the box and plaster was approximately of $4,7\,[kg]$. This load already creates the near maximum auxetic behavior for this small sample. Therefore, this precluded comparing the coefficient of friction for a small normal load, without auxetic effect, with that for a larger normal load, with auxetic effect.
The classical experiment with boxes and small samples was not interesting in this case, due to the constraints of the machine. Other solutions had to be found.

Ideally, this experiment should be done with bigger samples, without using the top and bottom boxes. The large rough surface was placed and blocked on the bottom moving recipient, as visible in figure 31. Since there is no top box to be attached to the fixed part, a way had to be found to hang the sample directly. It was decided to put the sample upside down in the mold which is much stiffer and allows a uniform stress distribution. A string was attached around the mold, as seen in Figure 31.

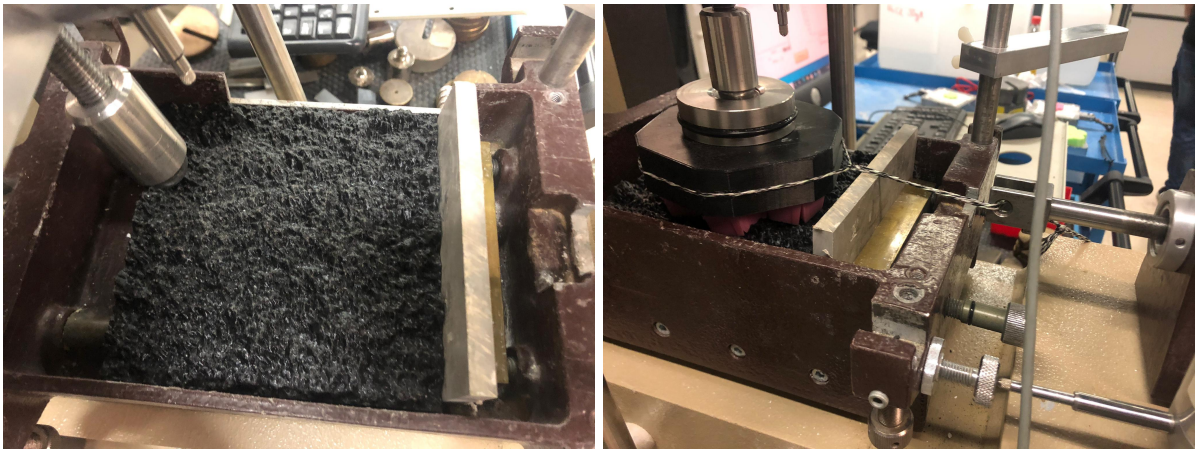

Figure 31: Set-up for the bigger sample

Other problems occurred when the test began that prevented any result to be obtained. The maximum displacement of the machine is about 13 mm, which is lower than the possible internal deformation of the sample when submitted to shear deformation, between its top and bottom part. The whole deformation was therefore internal to the element and there was no displacement between the sample and the rough surface. The tangential force could not be measured, making the experiment obsolete.

At that point, a hybrid solution that would allow the acquisition of some results was necessary. With the large sample testing, the fact that the experiment was possible without the top box became apparent. Therefore, the large sample and the large surface were replaced by the small sample with the small surface, without the top box. The problem this time was, that with a very low normal load, the string pulling directly on the mold induced a tilt instead of an horizontal displacement, in the same way as for the simple test above . To counteract this, a clamping ring was placed around the mold, creating an extremely rigid circular element, and the string was attached to the clamping ring. The assembly can be seen in Figure 32.

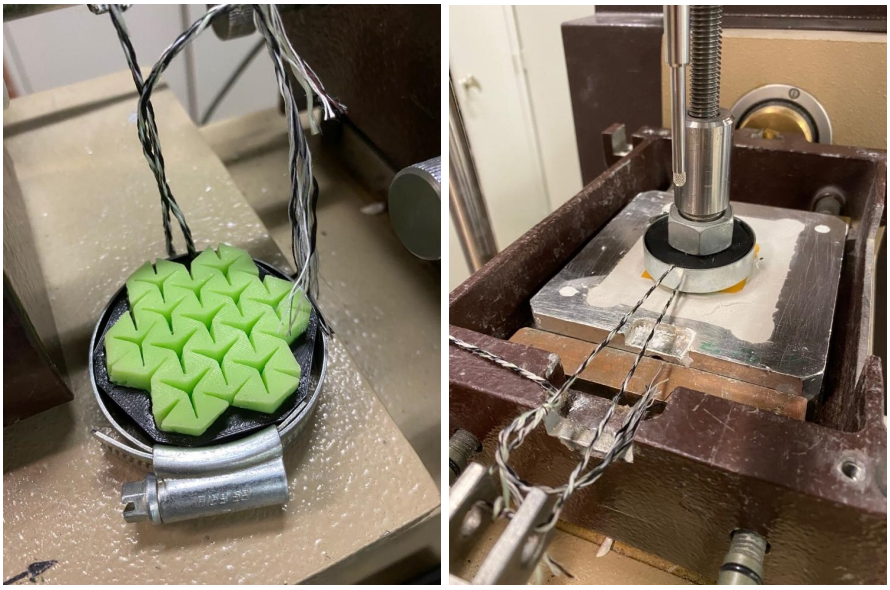

Figure 32: Final set-up

The experiment could then be performed for different normal loads, both on a rough surface and on a flat surface. As the loads increase very quickly, the sample made with the green resin was chosen as being more rigid and therefore more interesting for this type of experiment. An example of the test can be seen in figure 33

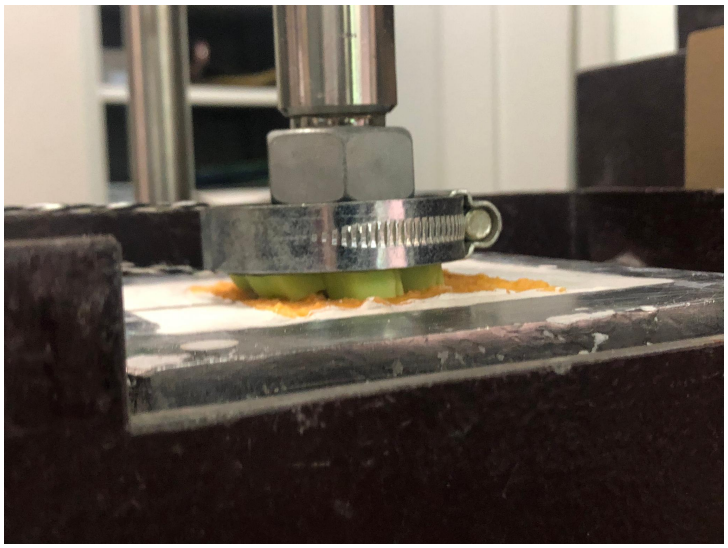

Figure 33: Exemple of experience

These different experiments allowed us to obtain different normal force - tangential force relationships, both statically and dynamically. These results needs to be analysed and interpreted.

6.3.4 Results and interpretation

The test allows a certain amount of information to be obtained continuously, for example the evolution of the tangential force or displacement as a function of time. The tangential force increases to a peak value which corresponds to the first movement between the sample and the surface. It will then stabilise at a residual value corresponding to the sample already in motion. This means that for each normal force, two corresponding tangential forces can be obtained.
The first one corresponds to the tangential force necessary to create the first movement. This will allow the static friction coefficient to be determined.
The second is the tangential force required when the sample is already in motion. It is therefore a plateau that will be lower than the previous peak tangential force. This makes it possible to determine a dynamic friction coefficient.

The following two relationships can be used to determine the friction coefficients.

$$\mu_s = \frac{T_{peak}}{N} \tag{15}$$

$$\mu_c = \frac{T_{res}}{N} \tag{16}$$

Where T_{peak} is the maximum tangential force and T_{res} is the residual tangential force in motion; N being the normal force applied.

Note : In general, the start of the sample movement on the surface takes place after about 6 mm of box movement, as it is seen on Figure 34. As explained earlier, at first, the sample deforms itself. As with the small sample, it takes about 6 mm to have the first displacement and the maximum displacement of the machine is 13 mm, it is easy to understand that there was not enough displacement of the machine to have interesting results with the large element.

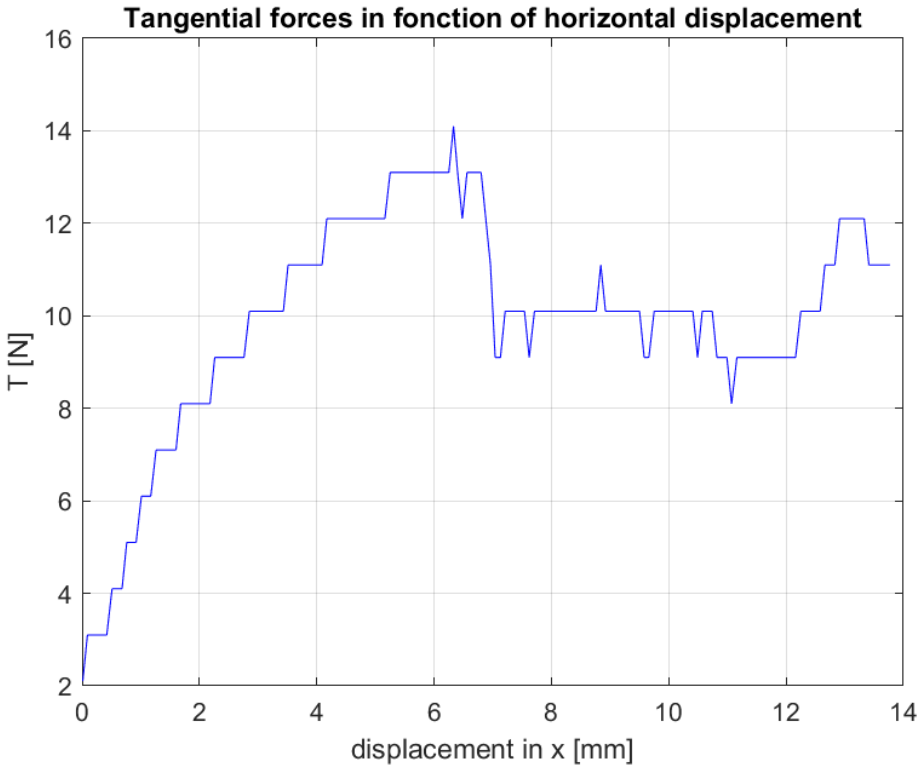

Figure 34: Tangential force in function of displacement

The interest of this experiment is to see if auxetism will tend to increase the coefficient of friction. It is therefore possible to run a linear regression on the different data sets available (smooth and rough surface, tangential force for the static and dynamic coefficient). The idea is to make graphs of normal force-tangential force and see if the relationship seems rather linear or not. The slope of the linear regression line that best interpolates the data then corresponds to the static (respectively dynamic) friction coefficient. The different results can be seen in figure 35 and table 5

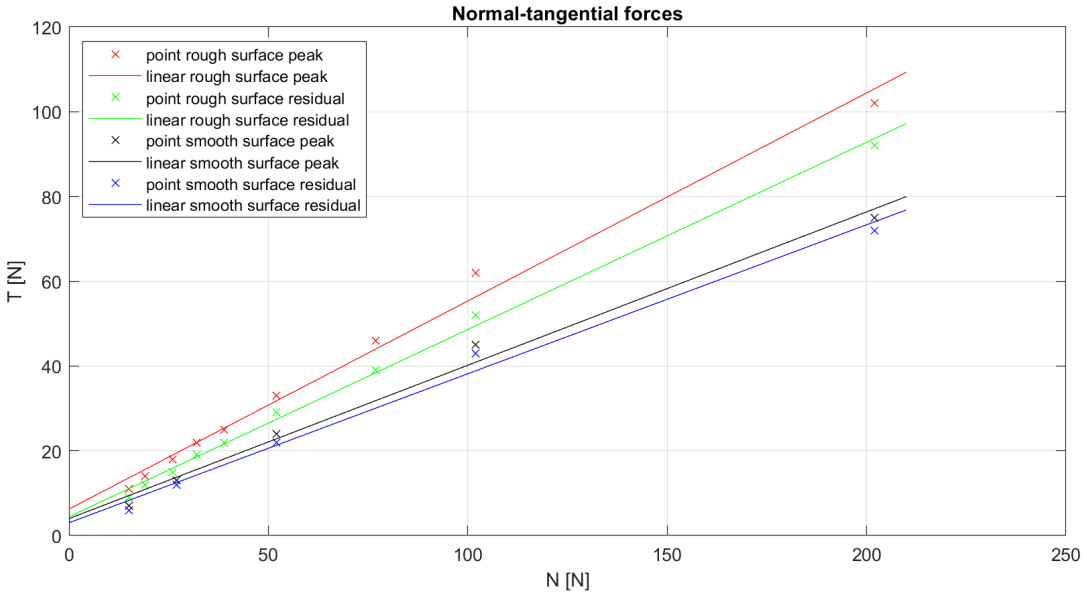

Figure 35: Relation Normal-Tangential forces

	μ_s	μ_c	intercept	r_{value}	p_{value}	std_{err}
rough surface static	0.491	-	6.23	0.996	$1.77 \cdot 10^{-8}$	0.0174
rough surface dynamic	-	0.442	4.42	0.998	$5.66 \cdot 10^{-8}$	0.0095
smooth surface static	0.362	-	4.00	0.995	$3.92 \cdot 10^{-4}$	0.0204
smooth surface dynamic	-	0.351	3.02	0.995	$3.87 \cdot 10^{-4}$	0.0198

Table 5: Interpolation parameters

Note: For the interpretation of the values, the p-value corresponds to a probability of linkage, the closer it is to 0, the more confidently it can be stated that there is a relationship between the data and the type of model chosen. Generally in statistics, a value of less than 0.05 is accepted as a reference. For the R-value, the closer the value is to 1, the better the interpolation of the data is.

Looking at the graphs, there seems to be an almost linear relationship between the tangential force and the normal force, both for the smooth and rough surface and for the peak and residual values.
Looking more closely at the statistical coefficients of the different linear regressions shown in Table 5, the initial intuition seems to be confirmed. The p-values are close to 0 and the r-values are close to 1, which shows that the linear regression fits rather well the data measured in the different experiments.

However, this initial feeling needs to be qualified. Indeed, the interception values should, in theory, be equal to 0 since there should be no tangential force if the normal force is strictly zero. This is not possible in practice as there is always some elemental weight acting as a normal force but it shows that the regression is not perfect. Moreover, the predominant observation is rather that of a very slight decrease of the friction coefficient with the increase of the normal force, when the opposite was rather expected. Indeed, when the normal force increases, the stars tend to close and auxetism appears. The hypothesis was that this would tend to cling better to the various asperities of the surface and thus increase the value of the friction coefficient.

Since this does not seem to be the case in practice, it is necessary to try to understand this result. There are several possible reasons for this:

1. The machine used is not perfectly suited for low load testing as it is normally designed for rocks. The experiment had to be adapted to avoid using the top box, which is not ideal.

2. The machine's sensor is also an officer-capable sensor for large loads. On the other hand, it is not designed to have a high accuracy for small forces. This is not a problem for normal large loads but may be important in this case.

3. The adaptations that had to be made to avoid using the top box can be quite inaccurate. Indeed, this involved the use of a string which is likely to transmit the force less well when the tangential, and therefore normal force, increases. The clamping ring and the mold are also not necessarily perfect solutions to get the real behaviour. In the end, the addition of all these components can have the effect of masking the auxetic behaviour as the measurement becomes less and less accurate with increasing forces.

4. It is also possible that the behaviour imagined is not the behaviour observed in practice. Indeed, the compression test shows that the desired behaviour, i.e. the closing of the stars, does take place under a sufficient normal load, but there is no evidence that this will tend to increase the coefficient of friction with certainty. The finite element test could be partially verified in practice as there was some auxeticism in both cases, but there is no evidence at present that the coefficient of friction is actually increased.

In order to get a more precise idea of the real properties that this auxetic behaviour can offer, it will be necessary to carry out other more suitable or more complete tests. Indeed, in view of the points listed above and the various uncertainties, it is complicated to have a definitive opinion on the properties of auxetic materials.

Several options can be considered. First of all, the most reliable solution would be to carry out the tests with other machines, which are more suitable than machines designed for rock testing. Indeed, this would allow a test to be carried out without the need for a set-up adaptation. The results would then be subject to much less uncertainty and could be interpreted with more confidence.

Secondly, if we assume that the same machine is always available, we must try to find solutions to reduce losses and uncertainties. If it is assumed that the upper box is still a problem due to its weight, the mounting of the element to the transducer to prevent it from moving with the lower box can be reviewed. The string used was clearly not the solution with the lowest dissipation of energy. A more suitable system with more rigid elements should be considered. The mold used on top to stiffen the edge seems to be a good solution, but there is a possible loss of the force transmission.

Finally, by using a much stiffer resin requiring a much higher normal force to activate the auxetic, the classic solution of the machine with the top box could be considered. The weight of the latter would no longer necessarily be critical in distinguishing a potential change in behaviour with the activation of auxetism and the results would probably be more reliable.

7 Conclusion

Auxetic in sport and especially for grip applications have a great potential. In the case of the Nike auxetic shoe, it was interesting to observe and characterize the auxetic behaviour of the sole. This sole structure is similar to the rotating (semi-)rigid structure which behaves as triangles rotating around hinges. However, compared to an auxetic metamaterial whose behaviour is analysed through a Poisson's ratio, the heterogeneous auxetic macro-cell analysis presents numerous difficulties.

A first parametrical design of the cell was done on Fusion 360 software. It allowed the modification of the cell based for example on the star-shaped void arm length, or even its height or opening. After verifying the cell behaviour described on Nike patent through a FEM analysis, these last three parameters values were modified, and the new auxetic cell was studied, to better understand how to characterize the behaviour of the sole auxetism. With three different methods, it turns out this characterization presents complications and the results should be open to a discussion. It was found that with an increasing void opening (center distance - bottom), the star-closing effect is increased. The same goes for a longer star arm with the constraint of the width of the hinge being sufficient not to have extreme load concentrations. For the void height, the optimal auxetic effect was found for a minimal ratio (void height compared to the length of the hexagon side) of $VH_{opt,min} \cong 0.875$.

After conducting a FEM analysis, molds were printed and 3D samples were casted with two different silicones. This allowed real tests to be performed, firstly to verify the auxetic behaviour and secondly to characterize the grip of such cells. It was found that for a compression test, the desired behaviour, i.e. closing the stars, was observed. This confirms the description of the patent as well as the observations made on the finite element tests. The resulting intuition is that this increase in surface area under normal load could have the effect of increasing the grip of the element. Friction coefficient tests were therefore carried out. However, the various approximations mentioned above, added to a seemingly imprecise test, prevent from having totally reliable results. At first sight, there is no increase in the coefficient of friction with normal load and thus no exhibition of auxetism. However, tests with more adapted machines or adaptations of the current experiment should be carried out in order to present a clearer link between auxetism and grip.

8 Acknowledgements

We would like to thank Jean-François Molinari, Ghatu Subhash, John Kolinski, Sacha Wattel and Son Pham-Ba for their valuable help and the constant follow-up during all the course of this project. We would also like to thank Youssef Edderbbarh for his help in the sample creation and the 3D printing of the mold.

Jean-François Molinari proposing the subject and John Kolinski allowing us to use his laboratory equipment was also greatly appreciated.

Finally, for the use of the machines in the rock laboratory, we would like to thank Marie Violay and Laurent Gastaldo.

9 Appendix - Getting started with cRacklet

For the master project taking place next semester, patterned frictional surfaces will be studied. With cRackelt, that is a spectral boundary element method [7] (made from [8],[9],[10]), the behaviour of shear surfaces will be analysed in 2D or 3D. The code can be adpated to the future study. First, a Linux virtual machine had to be installed in order for the code to run. This C++ code is provided with a Python interface that allows a more intuitive interaction with the parameters and properties used for the interface.

Different patterns on the surface induce an heterogeneity of the interface that can be modelled by lower or higher fracture toughness. cRacklet can be used to model a mode II crack which stands for in-plane shear conditions but also to model a mode I crack which suppose tension perpendicular to the interface; in the study of patterned frictional surfaces, mixed mode (I and II) will be used. Through the tutorial "supershear transition of a frictional crack propagating along an heterogeneous interface" [7], mode II crack propagation is presented as an exemple of the possible analysis of cRacklet. Boundary element method is used; two elastic semi-infinite body that are driven by constant far-field load τ_0 are considered. An initial crack of dimension a_0 propagates; shear stresses and propagation speed can be computed on space-time diagrams.

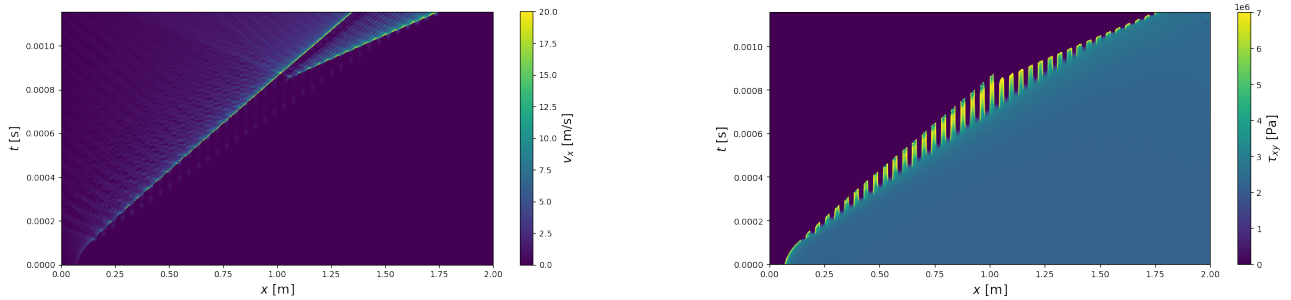

(a) Speed propagation of the crack

(b) Shear stresses

Figure 36: Space-time diagram obtained for the propagation of a crack on a heterogeneous surface [7]

As seen on Figure 36, different behaviours based on the asperities can be observed such as the formation of a second crack or the different intensities in shear stresses. This type of behaviour has a direct impact on friction and makes the study of patterned surface interesting.

In this code, different parameters can me modified such as the geometry and the material parameters. For the heterogeneous surface, different types of friction patterns will be studied. In the example of Figure 36, this is modelled by 50 patches of high and low fracture toughness. It will be interesting to see how to adapt the code to study for example the effect of crescent shaped asperities aswell as stick and slip behaviour.

References

[1] NIKE, Inc. The New Dimensions of Nike Free. https://news.nike.com/news/nike-free-2016-running-training, 2016. Accessed: 17.03.2021.

[2] T.M. Cross ; K.W. Hoffer ; D.P. Jones ; P.B. Kirschner ; E. Langvin ; J.C. Meschter. Auxetic structures and footwear with soles having auxetic structures, 2016. US 9.402.439 B2.

[3] H. M. A. Kolken and A. A. Zadpoor. Auxetic mechanical metamaterials. *RSC Advances*, 7(9):5111–5129, 2017.

[4] Autodesk. Fusion 360 - Integrated CAD, CAM, CAE and PCB software. https://www.autodesk.co.uk/products/fusion-360/overview?term=1-YEAR.

[5] Zhermack. Zhermack Elite double products. https://www.zhermack.com/en/product_category/dental/laboratory-dental-en/model-preparation/duplication/.

[6] L. Frérot ; G. Anciaux ; V. Rey ; S. Pham-Ba ; J-F. Molinari. Tamaas - A high-performance library for periodic rough surface contact. https://pypi.org/project/tamaas/.

[7] Barras F. ; Roch T. ; Spielmann D. ; Kammer D. ; Anciaux G. ; Richart N. ; Geubelle P.H. ; Molinari J.F. cRacklet. https://cracklet.gitlab.io/cracklet/quickstart.html.

[8] M. S. Breitenfeld and P. H. Geubelle. Numerical analysis of dynamic debonding under 2d in-plane and 3d loading. *International Journal of Fracture*, 93(1-4):13–38, 1998.

[9] P. H. Geubelle and M. S. Breitenfeld. Numerical analysis of dynamic debonding under anti-plane shear loading. *International Journal of Fracture*, 85(3):265–282, 1997.

[10] P. H. Geubelle and J. R. Rice. A spectral method for three-dimensional elastodynamic fracture problems. *Journal of the Mechanics and Physics of Solids*, 43(11):1791–1824, 1995.